## Interaction between hormone-sensitive lipase and ChREBP in fat cells controls insulin sensitivity

Morigny, Pauline; Houssier, Marianne; Mairal, Aline; Ghilain, Claire; Mouisel, Etienne; Benhamed, Fadila; Masri, Bernard; Recazens, Emeline; Denechaud, Pierre-Damien; Tavernier, Geneviève; Caspar-Bauguil, Sylvie; Virtue, Sam; Sramkova, Veronika; Monbrun, Laurent; Mazars, Anne; Zanoun, Madjid; Guilmeau, Sandra; Barquissau, Valentin; Beuzelin, Diane; Bonnel, Sophie; Marques, Marie; Monge-Roffarello, Boris; Lefort, Corinne; Fielding, Barbara; Sulpice, Thierry; Astrup, Arne; Payrastre, Bernard; Bertrand-Michel, Justine; Meugnier, Emmanuelle; Ligat, Laetitia; Lopez, Frédéric; Guillou, Hervé; Ling, Charlotte; Holm, Cecilia; Rabasa-Lhoret, Remi; Saris, Wim H M; Stich, Vladimir; Arner, Peter; Rydén, Mikael; Moro, Cedric; Viguerie, Nathalie; Harms, Matthew; Hallén, Stefan; Vidal-Puig, Antonio; Vidal, Hubert; Postic, Catherine; Langin, Dominique

Nature Metabolism

Publication date: 2019

Document version Peer reviewed version

Citation for published version (APA):

Morigny, P., Houssier, M., Mairal, A., Ghilain, C., Mouisel, E., Benhamed, F., ... Langin, D. (2019). Interaction between hormone-sensitive lipase and ChREBP in fat cells controls insulin sensitivity. *Nature Metabolism*, *1*(1), 133-146.



## Interaction between Hormone-Sensitive Lipase and ChREBP in Fat Cells Controls Insulin Sensitivity

Pauline Morigny, Marianne Houssier, Aline Mairal, Claire Ghilain, Etienne Mouisel, Fadila Benhamed, Bernard Masri, Emeline Recazens, Pierre-Damien Denechaud, Geneviève Tavernier, et al.

### ▶ To cite this version:

Pauline Morigny, Marianne Houssier, Aline Mairal, Claire Ghilain, Etienne Mouisel, et al.. Interaction between Hormone-Sensitive Lipase and ChREBP in Fat Cells Controls Insulin Sensitivity. Nature Metabolism, Nature Publishing Group, 2019, 1 (1), pp.133-146. 10.1038/s42255-018-0007-6 . inserm-02150261

### HAL Id: inserm-02150261 https://www.hal.inserm.fr/inserm-02150261

Submitted on 7 Jun2019

**HAL** is a multi-disciplinary open access archive for the deposit and dissemination of scientific research documents, whether they are published or not. The documents may come from teaching and research institutions in France or abroad, or from public or private research centers. L'archive ouverte pluridisciplinaire **HAL**, est destinée au dépôt et à la diffusion de documents scientifiques de niveau recherche, publiés ou non, émanant des établissements d'enseignement et de recherche français ou étrangers, des laboratoires publics ou privés.

- Interaction between Hormone-Sensitive Lipase and ChREBP in Fat Cells
   Controls Insulin Sensitivity
- 3

Pauline Morigny<sup>1,2,26</sup>, Marianne Houssier<sup>1,2,26</sup>, Aline Mairal<sup>1,2</sup>, Claire Ghilain<sup>1,2</sup>, Etienne 4 Mouisel<sup>1,2</sup>, Fadila Benhamed<sup>3,4,5</sup>, Bernard Masri<sup>1,2</sup>, Emeline Recazens<sup>1,2</sup>, Pierre-Damien 5 Denechaud<sup>1,2</sup>, Geneviève Tavernier<sup>1,2</sup>, Sylvie Caspar-Bauguil<sup>1,2,6</sup>, Sam Virtue<sup>7</sup>, Veronika 6 Sramkova<sup>1,2,8,9</sup>, Laurent Monbrun<sup>1,2</sup>, Anne Mazars<sup>1,2</sup>, Madiid Zanoun<sup>1,2</sup>, Sandra Guilmeau<sup>3,4,5</sup>, 7 Valentin Barquissau<sup>1,2</sup>, Diane Beuzelin<sup>1,2</sup>, Sophie Bonnel<sup>1,2,9</sup>, Marie Marques<sup>1,2,9</sup>, Boris 8 Monge-Roffarello<sup>1,2</sup>, Corinne Lefort<sup>1,2</sup>, Barbara Fielding<sup>10</sup>, Thierry Sulpice<sup>11</sup>, Arne Astrup<sup>12</sup>, 9 Bernard Payrastre<sup>1,2</sup>, Justine Bertrand-Michel<sup>1,2</sup>, Emmanuelle Meugnier<sup>13</sup>, Laetitia Ligat<sup>14</sup>, 10 Frédéric Lopez<sup>14</sup>, Hervé Guillou<sup>15,16</sup>, Charlotte Ling<sup>17</sup>, Cecilia Holm<sup>18</sup>, Remi Rabasa-11 Lhoret<sup>19,20,21</sup>, Wim H. M. Saris<sup>22</sup>, Vladimir Stich<sup>8,9</sup>, Peter Arner<sup>23</sup>, Mikael Rydén<sup>23</sup>, Cedric 12 Moro<sup>1,2,9</sup>, Nathalie Viguerie<sup>1,2,9</sup>, Matthew Harms<sup>24</sup>, Stefan Hallén<sup>24</sup>, Antonio Vidal-Puig<sup>7,25</sup>, 13 Hubert Vidal<sup>13</sup>, Catherine Postic<sup>3,4,5</sup>, Dominique Langin<sup>1,2,6,9\*</sup> 14

15

<sup>16</sup> <sup>1</sup> Institut National de la Santé et de la Recherche Médicale (Inserm), UMR1048, Institute of

17 Metabolic and Cardiovascular Diseases, Toulouse, France;

18 <sup>2</sup> University of Toulouse, UMR1048, Institute of Metabolic and Cardiovascular Diseases,

19 Paul Sabatier University, Toulouse, France;

20 <sup>3</sup> Institut National de la Santé et de la Recherche Médicale (Inserm), U1016, Institut Cochin,

- 21 Paris, France;
- <sup>4</sup>Centre National de la Recherche Scientifique (CNRS), UMR 8104, Paris, France;
- 23 <sup>5</sup> Université Paris Descartes, Sorbonne Paris Cité, Paris, France;
- <sup>6</sup> Toulouse University Hospitals, Laboratory of Clinical Biochemistry, Toulouse, France;

- <sup>25</sup> <sup>7</sup> University of Cambridge Metabolic Research Laboratories, Wellcome Trust-MRC Institute
- 26 of Metabolic Science, Addenbrooke's Hospital, Cambridge CB2 0QQ, UK;
- 27 <sup>8</sup> Department for the Study of Obesity and Diabetes, Third Faculty of Medicine, Charles
- 28 University, Prague, Czech Republic;
- 29 <sup>9</sup> Franco-Czech Laboratory for Clinical Research on Obesity, Third Faculty of Medicine,
- 30 Prague and Paul Sabatier University, Toulouse, France;
- <sup>10</sup> Department of Nutritional Sciences, University of Surrey, Guildford, Surrey;
- 32 <sup>11</sup> Physiogenex SAS, Prologue Biotech, Labège, France;
- 33 <sup>12</sup> Department of Nutrition, Exercise and Sports, Faculty of Science, University of
- 34 Copenhagen, Copenhagen, Denmark;
- 35 <sup>13</sup> CarMeN Laboratory, Inserm U1060, INRA U1397, Université Lyon 1, INSA Lyon,
- 36 Oullins, France;
- <sup>37</sup> <sup>14</sup> Pôle Technologique, Cancer Research Center of Toulouse (CRCT), Plateau Interactions
- 38 Moléculaires, INSERM-UMR1037, 31037 Toulouse, France.
- <sup>15</sup> Institut National de la Recherche Agronomique (INRA), UMR1331, Integrative Toxicology
- 40 and Metabolism, Toulouse, France
- 41 <sup>16</sup> University of Toulouse, UMR1331, Institut National Polytechnique (INP), Paul Sabatier
- 42 University, Toulouse, France;
- 43 <sup>17</sup> Department of Clinical Sciences, Epigenetics and Diabetes, Lund University Diabetes
- 44 Centre, Clinical Research Centre, Malmö, Sweden;
- <sup>45</sup> <sup>18</sup> Department of Experimental Medical Science, Lund University, Biomedical Centre, Lund,

46 Sweden;

- 47 <sup>19</sup> Institut de Recherches Cliniques de Montréal, Montreal, Canada;
- 48 <sup>20</sup> Department of nutrition, Université de Montréal, Montreal, Canada;
- 49 <sup>21</sup> Montreal Diabetes Research Center (MDRC), Montreal, Canada;

### Morigny, Houssier et al.

- 50 <sup>22</sup> Department of Human Biology, NUTRIM School of Nutrition and Translational Research
- 51 in Metabolism, Maastricht University Medical Centre, Maastricht, Netherlands;
- 52 <sup>23</sup> Department of Medicine, H7 Karolinska Institutet and Karolinska University Hospital,
- 53 Huddinge, Stockholm, Sweden;
- 54 <sup>24</sup> Cardiovascular, Renal and Metabolism, IMED Biotech Unit, AstraZeneca, Gothenburg,
- 55 Sweden;
- 56 <sup>25</sup> Wellcome Trust Sanger Institute, Wellcome Trust Genome Campus, Hinxton,
- 57 Cambridgeshire CB10 1SA, UK;
- 58 <sup>26</sup> These authors contributed equally to the work.
- 59
- 60 \*e-mail : dominique.langin@inserm.fr
- 61

### 62 ABSTRACT

63 Impaired adipose tissue insulin signaling is a critical feature of insulin resistance. Here we 64 identify a pathway linking the lipolytic enzyme, hormone-sensitive lipase (HSL), to insulin 65 action via the glucose-responsive transcription factor ChREBP and its target, the fatty acid 66 (FA) elongase, ELOVL6. Genetic inhibition of HSL in human adipocytes and mouse adipose 67 tissue results in enhanced insulin sensitivity and induction of ELOVL6. ELOVL6 promotes an 68 increase in phospholipid (PL) oleic acid which modifies plasma membrane fluidity and 69 enhances insulin signaling. HSL deficiency-mediated effects are suppressed by gene silencing 70 of ChREBP and ELOVL6. Mechanistically, physical interaction between HSL and 71 ChREBPa, independently of lipase catalytic activity, impairs ChREBPa translocation into the 72 nucleus and induction of ChREBPB, the transcriptionally highly active isoform strongly 73 associated to whole body insulin sensitivity. Targeting the HSL-ChREBP interaction may 74 allow therapeutic strategies for the restoration of insulin sensitivity.

### 76 Introduction

77 Insulin resistance is a pathogenic mechanism involved in a wide array of diseases. Besides the well-established early defect seen in type 2 diabetes, insulin resistance plays a role in the 78 79 development of cancers such as colorectal cancer, liver diseases associated with non-alcoholic 80 steatohepatitis, cardiovascular diseases or, reproductive dysfunction e.g., in polycystic ovary 81 syndrome. Insulin resistance is also a feature of aging-related disorders such as 82 neurodegenerative diseases e.g., in Alzheimer disease. Adipose tissue metabolism has 83 emerged as a major determinant of systemic insulin sensitivity. Genetic ablation of insulininduced glucose transport in fat causes systemic insulin resistance<sup>1</sup>. Direct manipulation of 84 85 the fat cell insulin signaling pathway in mice also supports the systemic importance of adipose tissue <sup>2-4</sup>. Defects in adipose insulin signaling have been reported in insulin resistant 86 and type 2 diabetic patients 5-8. In this context, improvement of adipose tissue insulin action 87 88 appears to be an important target for recovery of whole body systemic insulin sensitivity. 89 Glitazones, a well-known class of insulin sensitizers, act through modulation of fat cell insulin sensitivity <sup>9,10</sup>. Given their side-effects and subsequent withdrawal in many countries, there is 90 91 an unmet need of drugs targeting adipose tissue. Excessive circulating levels of fatty acids are 92 considered as important contributors to insulin resistance through development of fatty acidinduced lipotoxicity in insulin-sensitive tissues such as liver and skeletal muscle<sup>11</sup>. Lowering 93 94 of plasma non-esterified fatty acid levels through inhibition of fat cell lipolysis has been 95 proposed as an approach to improve insulin sensitivity. However, human data questions the 96 association between production of fatty acids from adipose tissue lipolysis and insulin resistance in obesity <sup>12</sup>. Partial deficiency in HSL (encoded by *LIPE*), one of the neutral 97 98 lipases expressed in adipocytes, results in improvement of whole body insulin sensitivity in 99 obese mice without changes in plasma fatty acid levels suggesting that other mechanisms than lipolysis are involved <sup>13</sup>. 100

Here, in a series of in vitro and in vivo studies in humans and mice, we identified a pathway linking HSL to insulin resistance through interaction with the glucose-responsive transcription factor ChREBP. The physical interaction between HSL and ChREBP impairs nuclear translocation and activity of the transcription factor. In fat cells, the lipogenic enzyme ELOVL6 is a preferential target of ChREBP. Inhibition of HSL promotes activity of ELOVL6 and enhances insulin signaling through enrichment of plasma membrane phospholipids in oleic acid.

108

# 109 Reduction in HSL expression promotes *de novo* lipogenesis and insulin signaling in 110 human adipocytes

111 In adipocytes differentiated from human multipotent adipose-derived stem (hMADS) cells <sup>14,15</sup>, HSL gene silencing (Supplementary Fig. 1a,b,c) increased insulin-stimulated glucose 112 113 transport (Fig. 1a), glucose oxidation (Fig. 1b) and glucose carbon incorporation into FA, i.e. 114 *de novo* lipogenesis (**Fig. 1c**). Insulin signaling was enhanced in adipocytes with decreased 115 HSL expression as shown by enhanced activating phosphorylations of insulin receptor 116 substrate 1 (IRS1-pY612) and V-Akt murine thymoma viral oncogene homolog 117 (AKT)/protein kinase B (AKT-pS473, AKT-pT308) after insulin treatment (Fig. 1d,e,f). 118 Phosphorylation of AS160, an AKT substrate regulating translocation of the insulin-sensitive 119 glucose transporter GLUT4, showed a trend similar to IRS1 and AKT phosphorylation (Fig. 120 1g). As adipose tissue *de novo* lipogenesis is associated with insulin sensitivity in humans <sup>16,17</sup>, we tested whether direct inhibition of *de novo* lipogenesis has an impact on the 121 122 modulation of insulin signaling induced by HSL depletion. To this end, human adipocytes were treated with a selective inhibitor of FA synthase, the rate-limiting enzyme in the 123 124 synthesis of palmitic acid (Supplementary Fig. 1d). The FA synthase inhibitor blunted the 125 induction of insulin-mediated phosphorylation of AKT observed in HSL-deficient fat cells

(Supplementary Fig. 1e). To further probe the role of *de novo* lipogenesis, we analyzed FA composition in fat cell triglycerides (TG) and PL. HSL inhibition significantly decreased the proportion of palmitic acid and palmitoleic acid but increased that of oleic acid in TG and PL (Fig. 1h,i).

130 To define the molecular mechanisms underlying the changes in FA composition, we analyzed 131 gene expression of enzymes catalyzing key steps in the synthesis of the main saturated and 132 monounsaturated FA derived from glucose in human fat cells (Supplementary Fig. 1d). In 133 hMADS adipocytes with decreased HSL expression, the most robust induction was observed 134 for *ELOVL6* (Fig. 1j). The increase in *ELOVL6* mRNA level was mirrored by an increase in 135 enzyme activity (Supplementary Fig. 1f) and an increase in the FA elongation ratio 136 attributable to ELOVL6 activity (Supplementary Fig. 1g). To confirm data from hMADS 137 adipocytes, we performed HSL gene silencing in human preadipocytes differentiated in 138 primary cultures. ELOVL6 also showed the highest induction among de novo lipogenesis 139 genes (Supplementary Fig. 1h). Next, we evaluated the effect of adipose triglyceride lipase 140 (ATGL encoded by PNPLA2), through ATGL gene silencing in hMADS adipocytes 141 (Supplementary Fig. 1i,j). ATGL precedes HSL in the sequential breakdown of TG during 142 adipocyte lipolysis. Contrarily to what is observed during HSL depletion, ATGL knock down 143 had no effect on *ELOVL6* and other *de novo* lipogenic enzyme mRNA levels as well as on the 144 FA elongation ratio attributable to ELOVL6 activity (Supplementary Fig. 1k,l). Altogether, 145 the results show that HSL depletion improves insulin signaling and, promotes de novo 146 lipogenesis and modification in FA composition. These changes are associated with induction 147 of the FA elongase ELOVL6.

148

149 HSL inhibition is associated with improved insulin sensitivity and increased adipose

150 tissue *Elovl6* expression in vivo

151 To probe changes in insulin sensitivity upon decreased HSL expression in vivo, we 152 investigated different mouse transgenic models, genetic backgrounds and diets. First, we 153 investigated B6D2/F1 transgenic mice with Lipe haploinsufficiency fed with 60% high fat 154 diet <sup>13</sup>. Compared to obese wild type littermates, the mice showed no differences in body 155 weight and fat mass (Supplementary Fig. 2a,b). During euglycemic hyperinsulinemic clamp, 156 the glucose infusion rate tended to increase (Fig. 2a) while there was no change in glucose 157 rate of disappearance in obese *Lipe* haploinsufficient mice compared with wild type 158 littermates (Fig. 2b). Insulin-mediated suppression of hepatic glucose production was 159 improved (Fig. 2c). In a second cohort of B6D2/F1 mice fed 45% high fat diet, insulin 160 tolerance was improved while body weight was not modified in *Lipe* haploinsufficient mice 161 compared with wild type littermates (Fig. 2d, Supplementary Fig. 2c). In a third cohort of 162 C57BL/6J mice fed 60% high fat diet, we confirmed enhanced insulin sensitivity in Lipe 163 haploinsufficient mice as determined by quantitative insulin-sensitivity check index 164 (QUICKI) (Fig. 2e). Adipose Elov16 gene expression was higher in mice with diminished 165 HSL expression (Fig. 2f). As in human adipocytes (Fig. 1j, Supplementary Fig 1h), the 166 induction was more pronounced for *Elovl6* than for other lipogenic genes (Supplementary 167 Fig. 2d).

168 To generate a mouse model with HSL knock down in adipose tissue and unaltered expression 169 in liver, we produced B6D2/F1 mice with zinc finger nuclease-mediated deletion of exon B 170 (Supplementary Fig. 2e). The promoter upstream of exon B governs HSL expression in fat cells <sup>18</sup>. *Lipe<sup>exonB-/-</sup>* mice showed decreased expression of HSL in adipose tissue (Fig. 2g,h). In 171 liver, the low levels of HSL which are mainly composed of exon A-containing transcripts, 172 were not modified (Supplementary Fig. 2f,g). Lipe<sup>exonB-/-</sup> mice fed high fat diet showed 173 improved glucose tolerance (Fig. 2i) without alteration of body weight (Supplementary Fig. 174 175 **2h**). Adipose *Elovl6* gene expression was higher in these mice compared to wild type littermates (Fig. 2j). Pharmacological inhibition of HSL had positive effect in C57BL/6J
mice. Chronic treatment with a specific inhibitor of HSL did not alter body weight
(Supplementary Fig. 2i) but resulted in increased QUICKI (Supplementary Fig. 2j) and
higher induction of adipose *Elovl6* gene expression (Supplementary Fig. 2k). Therefore,
both genetic and pharmacologic inhibition of HSL results in improved insulin sensitivity and
enhanced *Elovl6* expression in adipose tissue in vivo.

182

# Adipose ELOVL6 has a positive effect on insulin signaling and is associated with insulin sensitivity in vitro and in vivo

185 To determine whether ELOVL6 was involved in the improvement of insulin signaling when 186 fat cell HSL expression is diminished, we performed siRNA-mediated knockdown of 187 ELOVL6 in human adjocytes. Gene silencing led to a significant decrease in ELOVL6 188 mRNA level and activity (Supplementary Fig. 3a,b). The increases in IRS1 (Fig. 3a) and 189 AKT (Fig. 3b, Supplementary Fig. 3c) phosphorylation observed in HSL-deficient 190 adipocytes were abrogated following concomitant gene silencing of ELOVL6. To assess the 191 importance of Elovl6 on adipose tissue insulin signaling in vivo, a bolus of insulin was 192 injected to wild type and *Elovl6* null mice of similar body weights prior to collection and 193 analyses of fat pads (Supplementary Fig. 3d,e). In agreement with in vitro data in human 194 adipocytes, insulin-stimulated Akt phosphorylation was decreased in adipose tissue of *Elovl6* 195 null mice (Fig. 3c). These results reveal a strong link between ELOVL6 and insulin signaling 196 in fat cells and identify ELOVL6 as the mediator of the beneficial effects of HSL inhibition. 197 The relationship between adipose tissue ELOVL6 and insulin sensitivity was further explored

in mouse models and clinical cohorts. In mice fed high fat diet, the C57BL/6J strain showed higher insulin tolerance than DBA/2J strain (**Fig. 3d, Supplementary Fig. 3f**). The better insulin action in C57BL/6J mice was accompanied by higher induction of adipose tissue *Elovl6* gene expression during refeeding (**Fig. 3e**). In humans, *ELOVL6* gene expression was 202 first measured in visceral adipose tissue from lean insulin-sensitive individuals and obese 203 patients with metabolic syndrome, the latter being characterized by higher body mass index 204 and lower glucose disposal rate measured during euglycemic hyperinsulinemic clamp (Fig. 3f, 205 Supplementary Fig. 3g). Adipose tissue ELOVL6 mRNA levels were lower in insulin 206 resistant individuals (Fig. 3g). Additional evidence was provided by a longitudinal study. In 207 morbidly obese subjects, the weight loss observed two years after bariatric surgery 208 (Supplementary Fig. 3h) was associated with an improvement in insulin sensitivity 209 estimated by euglycemic hyperinsulinemic clamp-derived M value (Fig. 3h) and an increase 210 in subcutaneous adipose *ELOVL6* mRNA level (Fig. 3i). A strong positive correlation was 211 found between *ELOVL6* mRNA levels in subcutaneous fat and M value (Supplementary Fig. 212 **3i**). Taken together, both murine and human data show a positive association between adipose 213 ELOVL6 expression and insulin sensitivity in vivo.

214

## 215 ELOVL6 positive effect on insulin signaling is mediated by oleic acid content in PL and

### 216 plasma membrane fluidity

217 We sought to identify the mechanisms by which ELOVL6 improves insulin signaling. 218 Considering that the enzyme catalyzes critical steps in FA synthesis (Supplementary Fig. 219 1d), we investigated the direct contribution of ELOVL6 on the changes in fat cell FA 220 composition. In TG (Fig. 4a) and PL (Fig. 4b) of human adipocytes, diminished ELOVL6 221 expression led to an increase in palmitic acid and palmitoleic acid at the expense of oleic acid. 222 Analyses of these FAs were then performed on each class of PL. ELOVL6-deficient 223 adipocytes showed a decrease in the proportion of oleic acid (e.g., 36:2) and an increase in the 224 proportion of palmitic acid (e.g., 32:0) and palmitoleic acid (e.g., 32:2) in 225 phosphatidylcholines and phosphatidylethanolamines (Supplementary Fig. 4a-d). In 226 phosphatidylinositides, there was a decrease in 36:2 whereas no change was observed for

Morigny, Houssier et al.

227 phosphatidylserines. These findings were in agreement with in vivo data, where the lack of 228 Elovl6 in mouse adipose tissue resulted in increased palmitic and palmitoleic acid and 229 decreased oleic acid contents in adipose tissue (Supplementary Fig. 4e). The changes in FA 230 composition of PL suggest potential modification in plasma membrane properties. As 231 ELOVL6 mediates the positive effect of HSL gene silencing on insulin signaling (Fig. 3a,b, 232 Supplementary Fig. 3c), we determined whether this effect was dependent on oleic acid. 233 There are two enzymatic steps between palmitic acid and oleic acid (Supplementary Fig. 234 1d). The first is the elongation of palmitic acid into stearic acid catalyzed by ELOVL6 and the 235 second is the desaturation of stearic acid into oleic acid catalyzed by SCD, a highly active process in fat cells <sup>19-22</sup>. To investigate the respective contribution of the two steps, specific 236 inhibitors were used. Treatment of human adipocytes with an inhibitor of ELOVL6<sup>23</sup> resulted 237 in the expected changes in FA composition with a decrease of the C18/C16 FA ratio (Fig. 4c). 238 239 Concordant with data obtained using gene silencing (Fig. 3b), pharmacological inhibition of 240 ELOVL6 abrogated the enhancement of insulin-induced AKT phosphorylation observed in HSL-deficient adipocytes (Fig. 4d). A specific SCD inhibitor <sup>24</sup> decreased C16 and C18 FA 241 242 desaturation (Fig. 4e) and had the same effect as the ELOVL6 inhibitor on AKT 243 phosphorylation (Fig. 4f). Our data suggest that SCD is necessary but does not play a rate-244 limiting role as does ELOVL6 in the improvement of insulin signaling induced by HSL 245 inhibition. Accordingly, SCD mRNA levels are much higher than ELOVL6 mRNA levels in 246 human adipocytes (Supplementary Fig. 4f). In additional experiments, the content of oleic 247 acid in PL was directly modified by incubation of adipocytes with the FA (Fig. 4g). Exposure 248 of HSL and ELOVL6 double deficient adipocytes to oleic acid rescued insulin-induced AKT 249 phosphorylation to levels comparable with that observed in fat cells with diminished HSL 250 expression (Fig. 4h). Therefore, the beneficial role of ELOVL6 on insulin signaling in human 251 adipocytes is mediated by modulation of oleic acid content.

252 The composition of FA in PL may influence insulin signal transduction through modification of plasma membrane properties <sup>19,25,26</sup>. To determine the consequence of ELOVL6-mediated 253 254 changes in PL FA composition on plasma membrane fluidity, overexpression of ELOVL6 in 255 human adipocytes was achieved using an adenoviral vector (Supplementary Fig. 4g,h). The 256 resulting increase in C18/C16 FA ratio (Fig. 4i) was associated with an increase in insulin-257 induced IRS1 phosphorylation (Fig. 4j). Fluorescence recovery after photobleaching (FRAP) 258 data were analyzed in cells overexpressing ELOVL6 which plasma membrane glycolipids 259 were labeled by fluorescent cholera toxin subunit B (Fig. 4k). Comparison of the mobile 260 fractions (Fig. 41) revealed an increase in plasma membrane lateral mobility of cholera toxin-261 bound glycolipids in ELOVL6-overexpressing adipocytes. Collectively, the data suggest that 262 enhanced adipocyte ELOVL6 activity increases the proportion of oleic acid in PL and 263 positively influences insulin signaling through modulation of plasma membrane fluidity.

264

# The glucose-responsive transcription factor ChREBP mediates the beneficial effect of diminished HSL expression through ELOVL6 induction

ELOVL6 is a direct transcriptional target of ChREBP<sup>27</sup>. Adipose ChREBP is a major 267 determinant of systemic insulin action on glucose metabolism <sup>28</sup>. Therefore, the direct 268 269 contribution of ChREBP to HSL gene silencing-mediated improvement of glucose 270 metabolism in human adjocytes was evaluated using RNA interference (Supplementary 271 Fig. 5a). During dual knockdown of HSL and ChREBP, the beneficial effects on glucose 272 metabolism observed in adipocytes with low HSL expression were diminished. Glucose 273 transport was decreased to control levels and the induction of *de novo* lipogenesis observed in 274 cells with single HSL knockdown was lowered in adipocytes with dual knockdown of HSL 275 and ChREBP (Fig. 5a,b). A similar pattern was observed for glucose and acetate carbon 276 incorporation into FA (Fig. 5b,c) showing that the upregulation of FA synthesis resulted not 277 only from increased glucose uptake but also from specific induction of *de novo* lipogenesis. 278 ChREBP gene silencing also mitigated the increase in insulin-induced IRS1 and AKT 279 phosphorylation (Fig. 5d,e). These results indicate that ChREBP is involved in the 280 improvement of glucose metabolism and insulin signaling induced by HSL downregulation. 281 Similarly to what had been observed for ELOVL6 knock down (Fig. 4a,b), ChREBP gene 282 silencing led to an increase in palmitic acid and palmitoleic acid and a decrease of oleic acid 283 (Fig. 5f,g). Accordingly, ChREBP gene silencing potently suppressed ELOVL6 gene 284 expression but had weak or no effect on other lipogenic genes suggesting that ELOVL6 is a 285 preferential target of ChREBP in human fat cells (Fig. 5h). The involvement of ChREBP in 286 adipose *Elovl6* gene expression was confirmed in vivo. In adipose tissue of *Mlxipl* null mice 287 (Supplementary Fig. 5b), *Elovl6* was the lipogenic gene which expression was the most 288 severely impaired (Fig. 5i).

289 Two isoforms of ChREBP have been identified. ChREBP $\alpha$ , which transcriptional activity is 290 regulated by glucose, and ChREBPB, a transcriptionally superactive and unstable isoform which is a direct transcriptional target of ChREBP $\alpha^{28,29}$ . We characterized the human  $\beta$ -291 specific exon of *MLXIPL* which extends 29 deoxynucleotides 3' of its mouse counterpart<sup>28</sup> 292 293 (Supplementary Fig. 5c). In human adipocytes with siRNA-mediated knock down of HSL, 294 the levels of *ChREBP* transcripts, notably the  $\beta$  isoform, were increased (Fig. 5j). 295 Recruitment of ChREBP on the functional carbohydrate response element (ChoRE) in the 296 *ELOVL6* promoter was investigated using chromatin immunoprecipitation assays<sup>27</sup>. In 297 hMADS adjpocytes, more binding events were detected on the ELOVL6 ChoRE than on 298 positive control regions in RORC and TXNIP, a well characterized target of ChREBP 299 (Supplementary Fig. 5d). ChREBP recruitment onto the *ELOVL6* promoter was markedly 300 enhanced in HSL-deficient compared to control adipocytes (Fig. 5k).

301 Interestingly, *ELOVL6* was strongly associated with *ChREBP* $\beta$  gene expression in human 302 hMADS adipocytes (Fig. 51) and human differentiated primary preadipocytes 303 (Supplementary Fig. 5e). Albeit less potent, a positive correlation was also found between 304 *ELOVL6* and *ChREBP* $\alpha$  (Supplementary Fig. 5f). Similarly, a highly significant correlation 305 between *ELOVL6* and *ChREBPB* was observed in human subcutaneous adipose tissue 306 samples (Fig. 5m). Short term elevation in plasma glucose and insulin levels during a 307 hyperglycemic hyperinsulinemic clamp led to a pronounced induction of adipose  $ChREBP\beta$ 308 (Fig. 5n) and *ELOVL6* (Fig. 5o) gene expression, illustrating the importance of glucose flux 309 into the fat cells in the control of *ELOVL6* expression in humans. Altogether, our results show 310 that ChREBPß mediates the effect of HSL deficiency on glucose metabolism and insulin 311 signaling through transcriptional activation of *ELOVL6*.

312

#### 313 HSL modifies ChREBP activity in fat cells through protein-protein interaction

314 As HSL catalyzes one of the rate-limiting steps in fat cell TG hydrolysis, we investigated 315 whether lipolysis per se contributed to the induction of ChREBP. Several lines of evidence 316 suggest that this is not the case. In the culture conditions used to study *de novo* lipogenesis, 317 the release of glycerol and FA in the culture medium was low and was not influenced by HSL 318 gene silencing (Supplementary Fig. 6a,b). Adipocytes were then treated with triacsin C, a potent inhibitor of long chain fatty acyl CoA synthetase <sup>14</sup>. If FAs were involved, enhanced 319 320 FA levels due to blockade of FA re-esterification should influence ChREBP and ELOVL6 321 induction in adipocytes with HSL knock down. However, the upregulation of ChREBP 322 isoform and ELOVL6 mRNA was not influenced by the treatment (Supplementary Fig. 6c-323 e). These data show that the lipolytic activity of HSL does not contribute to the induction of 324 ChREBP.

325 These findings led us to hypothesize that physical interaction between HSL and ChREBP may 326 influence ChREBP activity. HEK293 cells were transfected with vectors expressing HSL and ChREBP $\alpha$  with FLAG epitope tag <sup>30</sup>. Immunoprecipitation of cell lysates with anti-FLAG 327 328 IgG and immunoblotting with anti-HSL antibody showed that HSL co-immunoprecipitated 329 with ChREBPa (Supplementary Fig. 6f). Co-immunoprecipitation was observed using 330 FLAG-ChREBP immobilized on magnetic beads and recombinant HSL (Fig. 6a). Surface 331 plasmon resonance assays supported a direct binding between ChREBPa and HSL (Fig. 6b). 332 Interaction between endogenous proteins in adipocvtes was shown through 333 immunoprecipitation with anti-ChREBP and anti-HSL antibodies (Fig. 6c, Supplementary 334 Fig. 6g). In line with the lack of effect on *de novo* lipogenesis (Supplementary Fig. 1k,l), 335 ATGL displayed no interaction with ChREBPa further indicating that HSL interaction with 336 ChREBP $\alpha$  is independent lipolysis and specific to this neutral lipase (**Fig. 6c**).

337 Furthermore, interaction of HSL with ChREBPa was shown using in situ proximity ligation 338 assays using a pair of primary antibodies raised in two different species and a pair of secondary antibodies coupled to oligodeoxynucleotides <sup>31</sup>. Specific and robust fluorescence 339 340 signals were observed in the cytosol of fat cells from subcutaneous adipose tissue 341 (Supplementary Fig. 6h). Such signals were also seen in differentiated hMADS adipocytes 342 (Supplementary Fig. 6i). Little signal was detected in undifferentiated fibroblasts which do 343 not express HSL. Negative controls using incomplete sets of antibodies and assays using anti-344 ATGL and anti-AKT combined with anti-ChREBP antibodies supported specificity of the 345 interaction (Supplementary Fig. 6j,k). Human HepG2 hepatocytes which express significant 346 level of ChREBP but minute amounts of HSL showed few fluorescent spots (Supplementary 347 **Fig. 61,m**). Respective expression of ChREBP $\alpha$  and HSL in mouse tissues is coherent with a 348 fat-specific interaction of the two proteins (Supplementary Fig. 6n). The data suggest that 349 ChREBP $\alpha$  interaction with HSL is specific to fat cells.

Morigny, Houssier et al.

350 In mouse adipose tissue, co-immunoprecipitation between HSL and ChREBP was diminished 351 in *Lipe* haploinsufficient mice (**Fig. 6d**). In human adipocytes, HSL binding to ChREBP $\alpha$  was 352 reduced in cytoplasm when HSL expression was diminished using siRNA (Fig. 6e, 353 Supplementary Fig. 7a). This resulted in modification of ChREBP cellular distribution. 354 Compared to control cells, adipocytes with low HSL expression showed higher 355 immunofluorescence of ChREBP in nuclei indicating that ChREBPa nuclear translocation is 356 facilitated when interaction with HSL is diminished (Fig. 6f). Subcellular fractionation 357 confirmed an increased nuclear translocation in human adipocytes and mouse adipose tissues 358 with low HSL expression whereas no significant differences was observed in the cytosolic 359 fraction (Fig. 6g,h, Supplementary Fig. 7b,c). In mice, there was no difference in ChREBP $\alpha$ 360 protein content in fat pads of the two genotypes (Supplementary Fig. 7d). To evaluate the 361 effect of HSL on ChREBPa transcriptional activity, HEK293 cells were transfected with a 362 vector containing the luciferase reporter gene under the control of a promoter containing functional ChoREs<sup>32</sup>. Promoter activity increased when cells expressed ChREBPa and 363 364 decreased when cells co-expressed increasing amounts of HSL (Fig. 6i, Supplementary Fig. 365 **7e**). The data suggest that HSL binds to ChREBP $\alpha$  and sequesters the transcription factor in 366 the cytoplasm. Upon decrease of HSL expression, HSL-ChREBP interaction is diminished, 367 ChREBP $\alpha$  nuclear translocation is facilitated and its transcriptional activity is enhanced as 368 shown here in reporter gene assays and above in chromatin immunoprecipitation analysis 369 (Fig. 5k).

When HEK293 cells expressing HSL and ChREBP were treated with a HSL inhibitor, less interaction between HSL and ChREBP was observed (**Supplementary Fig. 7f**). In human adipose tissue, we previously identified a short form of HSL produced by in-frame skipping of exon 6 (**Supplementary Fig. 2e**) <sup>33,34</sup>. As exon 6 encodes the catalytic site Serine, HSL short form is devoid of enzymatic activity (**Supplementary Fig. 7g**). Expressed in HEK293 375 cells, HSL short form retained the capacity to bind ChREBP (Fig. 6j). An adenovirus 376 expressing HSL short form was used to transduce human adipocytes transfected with control or LIPE siRNA (Supplementary Fig. 7h). The induction of ELOVL6 in adipocytes with 377 378 diminished levels of HSL was blunted when HSL short form was expressed (Fig. 6k). A 379 similar pattern was observed for other *de novo* lipogenesis gene expression (Supplementary 380 Fig. 7i). The catalytically inactive form also reduced the increase in IRS1 phosphorylation 381 mediated by HSL down regulation (Fig. 61). Of note, the improvement of fat cell insulin 382 signaling was observed with no change in amount of ChREBP $\alpha$  protein in adipocytes 383 expressing HSL-S and in the absence of correlation between HSL and ChREBP $\alpha$  levels. 384 (Supplementary Fig. 7j,k). Altogether, our data suggest that HSL plays an important role 385 besides the hydrolysis of lipids in fat cells, the repression of ChREBP activity via direct 386 interaction with the transcription factor (Supplementary Fig. 8).

387

### 388 Discussion

389 Considering the soaring incidence of diseases characterized by an insulin resistance state, 390 there is a lack of drugs acting on adipose tissue. Its specialized cells, the adipocytes, have great potential to be therapeutically targeted <sup>35</sup>. Partial inhibition of the fat cell neutral lipase, 391 392 HSL, alleviates insulin resistance without increasing body weight, two essential requirements for therapeutic interventions <sup>13</sup> (and present work). Evolution of plasma fatty acid level and 393 394 variation in insulin sensitivity was dissociated in this model. Here, we deciphered the 395 mechanisms behind HSL inhibition-mediated improvement of glucose metabolism and 396 identified interactions between prototypical metabolic pathways of the adipocyte. We show 397 that, independently of lipolysis and the enzyme catalytic activity, HSL physically interacts 398 with and inhibits the transcription factor ChREBP. ChREBP controls the FA elongase 399 ELOVL6 catalyzing a limiting step in oleic acid synthesis. The resulting increase in PL oleic 400 acid content modifies plasma membrane properties and improves insulin signaling.

Morigny, Houssier et al.

Adipose *de novo* lipogenesis is positively associated with systemic insulin sensitivity <sup>36,37</sup>. *De* 401 402 novo lipogenesis is under the control of the glucose-responsive transcription factor, ChREBP. 403 A positive association between insulin sensitivity and adipose ChREBP, notably, the transcriptionally superactive  $\beta$  isoform, has been reported <sup>16,28,38</sup>. In human adipocytes, we 404 405 show that knockdown of ChREBP counteracts the beneficial effects of HSL gene silencing on 406 insulin sensitivity. We identify the FA elongase ELOVL6 as the main target of ChREBP $\beta$  in 407 HSL-deficient adipocytes. In humans, *ELOVL6* expression in fat was lower in insulin resistant than in insulin sensitive subjects in line with previous reports <sup>16,39</sup>. Of note, in monozygotic 408 409 twin pairs discordant for type 2 diabetes, adipose *ELOVL6* is markedly lower in the affected twins <sup>40</sup>. Our results from bariatric surgery, a longitudinal intervention improving insulin 410 411 control of glucose metabolism, also supported the tight link between adipose ELOVL6 and 412 insulin sensitivity.

ELOVL6 catalyzes a critical step in the elongation of C16 FA <sup>22,41</sup>. In adipocytes, enhanced 413 414 ELOVL6 activity favored oleic acid synthesis while ELOVL6 knock down had the opposite 415 effect. Diets rich in olive oil improve insulin sensitivity at adipocyte and whole-body levels 416  $^{42,43}$ . This effect may contribute to the decreased incidence of type 2 diabetes in patients at risk 417 fed Mediterranean diets <sup>43</sup>. At the cellular level, monounsaturated fatty acids have been reported to protect from the damaging effect of palmitic acid on insulin signaling <sup>19,26</sup>. As 418 419 ELOVL6 induced an increase of oleic acid in major classes of PL, we postulated that it may alter plasma membrane fluidity owing to its conformational plasticity <sup>25,44,45</sup>. The plasma 420 421 membrane lateral mobility of glycolipids was increased in fat cells overexpressing ELOVL6. 422 We therefore propose that ELOVL6-mediated increase in PL oleic acid content improves fat 423 cell insulin signaling through alteration of plasma membrane properties. In mice, *Elovl6* 424 deficiency impaired white adipose tissue insulin signaling whereas the opposite or lack of alteration have previously been reported in the liver suggesting tissue-specific differences in
 ELOVL6-mediated modulation of insulin action <sup>41,46</sup>.

The role of HSL in human fat cell lipolysis is well established <sup>14,47</sup>. HSL is a multifunctional 427 enzyme with a broad range of substrates. Besides tri-, di- and monoglycerides, HSL is able to 428 hydrolyze other esters, such as cholesteryl and retinyl esters <sup>48</sup>. As ChREBP activity is 429 430 influenced by metabolites and other transcription factors in liver, it could be postulated that 431 products of HSL enzymatic activity directly or indirectly influence ChREBP-mediated modulation of gene transcription<sup>29</sup>. However, although we cannot rule out that, in some 432 433 conditions, upregulation of ChREBPa protein expression partially contributes to the 434 phenotype of adipocytes depleted in HSL, we bring a solid body of evidence that physical 435 interaction between HSL and ChREBPa controls the intracellular location and activity of the 436 transcription factor in fat cells. ATGL which catalyzes the first step in adipose tissue lipolysis 437 does not interact with ChREBP and does not modulate *de novo* lipogenesis gene expression. 438 Moreover, using a short inactive form of HSL lacking the catalytic site Serine, we could show 439 that the catalytic activity of HSL is dispensable for the interaction with ChREBP and 440 ChREBP-mediated effect on *ELOVL6* expression and insulin signaling. Noteworthy, our data provide a function to this naturally occurring form expressed in human adipose tissue <sup>33</sup>. A 441 442 specific HSL inhibitor was able to diminish the interaction between HSL and ChREBP and 443 enhance adipose *Elovl6* expression in mice. It may be hypothesized that the inhibitor binding 444 to the catalytic pocket induces conformational change partially disrupting HSL-ChREBP 445 interaction. The data suggest that small molecules may be designed and used to disrupt the 446 interaction. Reducing the interaction between HSL and ChREBP favors ChREBP nuclear 447 translocation and its transcriptional activity. This pathway provides a molecular basis to the 448 differential control of *de novo* lipogenesis in liver and adipose tissue. ChREBP is involved in the regulation of *de novo* lipogenesis in the two tissues <sup>29,49</sup>. However, the pathway is 449

450 generally considered as detrimental in the liver as it is activated during the development of 451 fatty liver disease whereas it is seen as beneficial in adipose tissue as the link with insulin 452 sensitivity has been shown both in clinical studies and in mouse models <sup>50</sup>. HSL is expressed 453 at much higher level in fat cells than in hepatocytes. Accordingly, interaction between HSL 454 and ChREBP is not found in human hepatocytes. Alleviation of HSL-mediated inhibition of 455 ChREBP activity may constitute a fat cell-specific mechanism to enhance *de novo* lipogenesis 456 and insulin signaling.

To conclude, our work identifies a pathway critical for optimal insulin signaling in fat cells which links the neutral lipase HSL to the glucose-responsive transcription factor ChREBP and its target gene, the FA elongase, ELOVL6. This constitutes a unique example of an enzyme involved in lipid metabolism which independently of its enzymatic activity inhibits the transcriptional activity of a glucose-responsive transcription factor through protein-protein interaction. Inhibition of the HSL-ChREBP interaction may constitute an adipose-specific strategy to reduce insulin resistance.

### 465 ACKNOWLEDGMENTS

The authors gratefully acknowledge Dr. Nicolas Venteclef (Centre de Recherche des Cordeliers, Paris, France) and Dr. Jérémie Boucher (AstraZeneca, Göteborg, Sweden) for critical reading and comments on the manuscript. Emilie Courty and Jean Personnaz participated in mouse studies during internship at I2MC. The GenoToul Animal Care, Anexplo, Imaging-TRI (especially, Dr. Frédérique Gaits-Iacovoni for helpful discussion) and Quantitative Transcriptomics facilities contributed to the work.

- 472 This work was supported by Inserm, Paul Sabatier University, Fondation pour la Recherche
- 473 Médicale (DEQ20170336720 to D.L.), Agence Nationale de la Recherche (ANR-12-BSV1-
- 474 0025Obelip and ANR-17-CE14-0015Hepadialogue to D.L.), Région Midi-Pyrénées (OBELIP
- 475 and ILIP projects to D.L.), FORCE/F-CRIN for clinical research on obesity, EU/EFPIA
- 476 Innovative Medicines Initiative Joint Undertaking (EMIF grant n° 115372 to P.A., A.V.P. and

477 D.L.) and AstraZeneca France (TALIP project to D.L.).

478

479 D.L. is a member of Institut Universitaire de France.

480

### 481 AUTHOR CONTRIBUTIONS

482 P.M. and M.H. share first authorship. P.M. and M.Ho. performed the majority of in vitro 483 experiments and analyzed data with the contribution of A.Mai., C.G., F.B., B.M., E.R.,

- to experiments and analyzed data with the contribution of Filinal, C.G., T.D., D.M., E.R.,
- 484 P.D.D., V.Sr., V.B., D.B., M.M., C.L., L.L., F.L. and M.Ha. P.M., M.Ho., E.Mo., G.T., S.V.,
- 485 L.M., S.G., B.M.-R., T.S., H.G., C.H., A.V.P. and C.P. performed and analyzed in vivo data
- 486 from mouse models. P.M., S.B., M.M., B.F., A.A., E.Me., C.L., R.R.L., W.S., V.St., P.A.,
- 487 M.R., N.V. and H.V. performed and analyzed in vivo data in human clinical studies. S.C.-B.,
- 488 S.V. and J.B.-M. analyzed lipidomics data. A.Maz. and M.Z. performed and analyzed FRAP

Morigny, Houssier et al.

- 489 experiments. B.P., C.M., N.V., S.H. and H.V. interpreted the data. P.M., M.Ho. and D.L.
- 490 conceived the study, interpreted the data and wrote the manuscript. D.L. supervised the study.
- 491
- 492 COMPETING INTERESTS STATEMENT
- 493 T.S. is an employee of Physiogenex. M.H. and S.H. are employees of AstraZeneca. The other
- 494 authors declare no competing financial and non-financial interests.
- 495

### 496 REFERENCES

- 497 1. Abel, E.D., *et al.* Adipose-selective targeting of the GLUT4 gene impairs insulin
  498 action in muscle and liver. *Nature* 409, 729-733 (2001).
- 499 2. Morley, T.S., Xia, J.Y. & Scherer, P.E. Selective enhancement of insulin sensitivity in
  500 the mature adipocyte is sufficient for systemic metabolic improvements. *Nat Commun*501 6, 7906 (2015).
- Shearin, A.L., Monks, B.R., Seale, P. & Birnbaum, M.J. Lack of AKT in adipocytes
  causes severe lipodystrophy. *Mol Metab* 5, 472-479 (2016).
- Softic, S., *et al.* Lipodystrophy Due to Adipose Tissue Specific Insulin Receptor
   Knockout Results in Progressive NAFLD. *Diabetes* (2016).
- 506 5. Rondinone, C.M., *et al.* Insulin receptor substrate (IRS) 1 is reduced and IRS-2 is the
  507 main docking protein for phosphatidylinositol 3-kinase in adipocytes from subjects
  508 with non-insulin-dependent diabetes mellitus. *Proc Natl Acad Sci U S A* 94, 4171509 4175 (1997).
- 6. Carvalho, E., Jansson, P.A., Nagaev, I., Wenthzel, A.M. & Smith, U. Insulin
  resistance with low cellular IRS-1 expression is also associated with low GLUT4
  expression and impaired insulin-stimulated glucose transport. *FASEB J* 15, 1101-1103
  (2001).
- 514 7. Frojdo, S., Vidal, H. & Pirola, L. Alterations of insulin signaling in type 2 diabetes: a
  515 review of the current evidence from humans. *Biochim Biophys Acta* 1792, 83-92
  516 (2009).
- 8. Nyman, E., *et al.* A single mechanism can explain network-wide insulin resistance in
  adipocytes from obese patients with type 2 diabetes. *J Biol Chem* 289, 33215-33230
  (2014).

520	9.	Hammarstedt, A., Sopasakis, V.R., Gogg, S., Jansson, P.A. & Smith, U. Improved
521		insulin sensitivity and adipose tissue dysregulation after short-term treatment with
522		pioglitazone in non-diabetic, insulin-resistant subjects. Diabetologia 48, 96-104
523		(2005).

- 524 10. Yki-Jarvinen, H. Thiazolidinediones. *N Engl J Med* **351**, 1106-1118 (2004).
- 525 11. Samuel, V.T. & Shulman, G.I. Mechanisms for insulin resistance: common threads
  526 and missing links. *Cell* 148, 852-871 (2012).
- 527 12. Karpe, F., Dickmann, J.R. & Frayn, K.N. Fatty acids, obesity, and insulin resistance:
  528 time for a reevaluation. *Diabetes* 60, 2441-2449 (2011).
- 529 13. Girousse, A., *et al.* Partial inhibition of adipose tissue lipolysis improves glucose
  530 metabolism and insulin sensitivity without alteration of fat mass. *PLoS Biol* 11,
  531 e1001485 (2013).
- 532 14. Bezaire, V., *et al.* Contribution of adipose triglyceride lipase and hormone-sensitive
  533 lipase to lipolysis in hMADS adipocytes. *J Biol Chem* 284, 18282-18291 (2009).
- 534 15. Barquissau, V., *et al.* White-to-brite conversion in human adipocytes promotes
  535 metabolic reprogramming towards fatty acid anabolic and catabolic pathways. *Mol*536 *Metab* 5, 352-365 (2016).
- 537 16. Eissing, L., *et al.* De novo lipogenesis in human fat and liver is linked to ChREBP538 beta and metabolic health. *Nat Commun* 4, 1528 (2013).
- Roberts, R., *et al.* Markers of de novo lipogenesis in adipose tissue: associations with
  small adipocytes and insulin sensitivity in humans. *Diabetologia* 52, 882-890 (2009).
- 541 18. Grober, J., *et al.* Characterization of the promoter of human adipocyte hormone-542 sensitive lipase. *Biochem J* **328**, 453-461 (1997).

- 543 19. Collins, J.M., Neville, M.J., Hoppa, M.B. & Frayn, K.N. De novo lipogenesis and 544 stearoyl-CoA desaturase are coordinately regulated in the human adipocyte and 545 protect against palmitate-induced cell injury. *J Biol Chem* **285**, 6044-6052 (2010).
- 546 20. Guillou, H., Zadravec, D., Martin, P.G. & Jacobsson, A. The key roles of elongases
  547 and desaturases in mammalian fatty acid metabolism: Insights from transgenic mice.
  548 *Prog Lipid Res* 49, 186-199 (2010).
- 549 21. Hodson, L. & Fielding, B.A. Stearoyl-CoA desaturase: rogue or innocent bystander?
  550 *Prog Lipid Res* 52, 15-42 (2013).
- 551 22. Ohno, Y., *et al.* ELOVL1 production of C24 acyl-CoAs is linked to C24 sphingolipid
  552 synthesis. *Proc Natl Acad Sci U S A* 107, 18439-18444 (2010).
- Nagase, T., *et al.* Synthesis and biological evaluation of a novel 3-sulfonyl-8azabicyclo[3.2.1]octane class of long chain fatty acid elongase 6 (ELOVL6) inhibitors. *J Med Chem* 52, 4111-4114 (2009).
- 556 24. Xin, Z., et al. Discovery of piperidine-aryl urea-based stearoyl-CoA desaturase 1
  557 inhibitors. *Bioorg Med Chem Lett* 18, 4298-4302 (2008).
- Antonny, B., Vanni, S., Shindou, H. & Ferreira, T. From zero to six double bonds:
  phospholipid unsaturation and organelle function. *Trends Cell Biol* 25, 427-436
  (2015).
- 561 26. Holzer, R.G., *et al.* Saturated fatty acids induce c-Src clustering within membrane 562 subdomains, leading to JNK activation. *Cell* **147**, 173-184 (2011).
- 563 27. Bae, J.S., Oh, A.R., Lee, H.J., Ahn, Y.H. & Cha, J.Y. Hepatic Elovl6 gene expression
  564 is regulated by the synergistic action of ChREBP and SREBP-1c. *Biochem Biophys*565 *Res Commun* 478, 1060-1066 (2016).
- 566 28. Herman, M.A., *et al.* A novel ChREBP isoform in adipose tissue regulates systemic
  567 glucose metabolism. *Nature* 484, 333-338 (2012).

- Filhoulaud, G., Guilmeau, S., Dentin, R., Girard, J. & Postic, C. Novel insights into
  ChREBP regulation and function. *Trends Endocrinol Metab* 24, 257-268 (2013).
  Stoeckman, A.K., Ma, L. & Towle, H.C. Mlx is the functional heteromeric partner of
  the carbohydrate response element-binding protein in glucose regulation of lipogenic
  enzyme genes. *J Biol Chem* 279, 15662-15669 (2004).
- 573 31. Soderberg, O., *et al.* Direct observation of individual endogenous protein complexes in
  574 situ by proximity ligation. *Nat Methods* 3, 995-1000 (2006).
- 575 32. Lou, D.Q., *et al.* Chicken ovalbumin upstream promoter-transcription factor II, a new
  576 partner of the glucose response element of the L-type pyruvate kinase gene, acts as an
  577 inhibitor of the glucose response. *J Biol Chem* 274, 28385-28394 (1999).
- 578 33. Laurell, H., *et al.* Species-specific alternative splicing generates a catalytically inactive
  579 form of human hormone-sensitive lipase. *Biochem J* 328 (Pt 1), 137-143 (1997).
- 34. Ray, H., *et al.* The presence of a catalytically inactive form of hormone-sensitive
  lipase is associated with decreased lipolysis in abdominal subcutaneous adipose tissue
  of obese subjects. *Diabetes* 52, 1417-1422 (2003).
- 583 35. Kusminski, C.M., Bickel, P.E. & Scherer, P.E. Targeting adipose tissue in the 584 treatment of obesity-associated diabetes. *Nat Rev Drug Discov* (2016).
- 585 36. Czech, M.P. Cellular basis of insulin insensitivity in large rat adipocytes. *J Clin Invest*586 57, 1523-1532 (1976).
- 587 37. Hoffstedt, J., Forster, D. & Lofgren, P. Impaired subcutaneous adipocyte lipogenesis
  588 is associated with systemic insulin resistance and increased apolipoprotein B/AI ratio
  589 in men and women. *J Intern Med* 262, 131-139 (2007).
- 590 38. Kursawe, R., *et al.* Decreased transcription of ChREBP-alpha/beta isoforms in
  591 abdominal subcutaneous adipose tissue of obese adolescents with prediabetes or early

- 592 type 2 diabetes: associations with insulin resistance and hyperglycemia. *Diabetes* 62,
  593 837-844 (2013).
- Soronen, J., *et al.* Adipose tissue gene expression analysis reveals changes in
  inflammatory, mitochondrial respiratory and lipid metabolic pathways in obese
  insulin-resistant subjects. *BMC Med Genomics* 5, 9 (2012).
- 597 40. Nilsson, E., *et al.* Altered DNA methylation and differential expression of genes
  598 influencing metabolism and inflammation in adipose tissue from subjects with type 2
  599 diabetes. *Diabetes* 63, 2962-2976 (2014).
- Matsuzaka, T., *et al.* Crucial role of a long-chain fatty acid elongase, Elovl6, in
  obesity-induced insulin resistance. *Nat Med* 13, 1193-1202 (2007).
- 42. Ryan, M., *et al.* Diabetes and the Mediterranean diet: a beneficial effect of oleic acid
  on insulin sensitivity, adipocyte glucose transport and endothelium-dependent
  vasoreactivity. *QJM* 93, 85-91 (2000).
- 43. Salas-Salvado, J., *et al.* Reduction in the incidence of type 2 diabetes with the
  Mediterranean diet: results of the PREDIMED-Reus nutrition intervention randomized
  trial. *Diabetes Care* 34, 14-19 (2011).
- 44. Ibarguren, M., *et al.* Partitioning of liquid-ordered/liquid-disordered membrane
  microdomains induced by the fluidifying effect of 2-hydroxylated fatty acid
  derivatives. *Biochim Biophys Acta* 1828, 2553-2563 (2013).
- 611 45. Pietilainen, K.H., *et al.* Association of lipidome remodeling in the adipocyte
  612 membrane with acquired obesity in humans. *PLoS Biol* 9, e1000623 (2011).
- 613 46. Moon, Y.A., Ochoa, C.R., Mitsche, M.A., Hammer, R.E. & Horton, J.D. Deletion of
- 614 ELOVL6 blocks the synthesis of oleic acid but does not prevent the development of 615 fatty liver or insulin resistance. *J Lipid Res* **55**, 2597-2605 (2014).

Morigny, Houssier et al.

- 47. Lafontan, M. & Langin, D. Lipolysis and lipid mobilization in human adipose tissue.
  617 *Prog Lipid Res* 48, 275-297 (2009).
- Kraemer, F.B. & Shen, W.J. Hormone-sensitive lipase: control of intracellular tri-(di)acylglycerol and cholesteryl ester hydrolysis. *J Lipid Res* 43, 1585-1594 (2002).
- 49. Postic, C. & Girard, J. Contribution of de novo fatty acid synthesis to hepatic steatosis
  and insulin resistance: lessons from genetically engineered mice. *J Clin Invest* 118,
  829-838 (2008).
- 50. Solinas, G., Boren, J. & Dulloo, A.G. De novo lipogenesis in metabolic homeostasis:
  More friend than foe? *Mol Metab* 4, 367-377 (2015).

### 626 FIGURE LEGENDS

627 Figure 1. Reduced HSL expression promotes glucose metabolism and insulin signaling in 628 human adipocytes. Experiments were carried out in control (white bars, siCTR) and HSL-629 deprived (grey bars, siHSL) hMADS adipocytes. (a-g) Adipocytes were analyzed in basal (-) 630 and insulin-stimulated (+, 100nM) conditions. (a) Glucose transport using radiolabelled 2-631 deoxyglucose (n=12 biologically independent samples per group) (Insulin stimulation: 632 P < 0.0001). (b) Glucose oxidation using radiolabelled glucose (n=10 biologically independent 633 samples per group) (Insulin stimulation: P=0.0015). (c) de novo lipogenesis using 634 radiolabelled glucose (n=10 biologically independent samples per group) (Insulin stimulation: 635 P<0.0001). (d-g) Insulin signaling evaluated by activating phosphorylation of IRS1 (pY612) 636 (n=7 biologically independent samples per group) (Insulin stimulation: P=0.0033) (d) AKT 637 (pS473) (n=5 biologically independent samples per group) (Insulin stimulation: P=0.0005) 638 (e), AKT (pT308) (n=8 biologically independent samples per group) (Insulin stimulation: 639 P=0.0201) (f) and AS160 (pT642) (n=4 biologically independent samples per group) (Insulin 640 stimulation: P=0.0726) (g). Size markers (in kDa) are shown on illustrative Western blot 641 panels. (h, i) Fatty acid composition in triglycerides (TG) (h) and phospholipids (PL) (i) (n=8 642 biologically independent samples per group). (j) mRNA levels of lipogenic enzymes (n=6 643 biologically independent samples per group). Data are mean ±sem. Statistical analysis was 644 performed using two-way ANOVA with Bonferroni's post hoc tests (a-g), paired Student's t 645 test (h, i) and Wilcoxon's test (j). Statistical tests were two-sided. \*P<0.05, \*\*P<0.01, 646 \*\*\*P<0.001 compared to control.

**Figure 2.** HSL inhibition is associated with increased insulin sensitivity and adipose tissue ELOVL6 expression *in vivo*. (**a-f**) Experiments were carried out in wild type (WT, white bars) and HSL haploinsufficient (*Lipe*<sup>+/-</sup>, grey bars) mice. (**a-c**) Glucose infusion rate (GIR) (**a**) post

651 insulin glucose rate of disappearance (Glucose Rd) (b) and hepatic glucose production (HGP) 652 (c) during euglycemic-hyperinsulinemic clamp in B6D2/F1 mice fed 60% high fat diet for 3 months (WT n=7 animals,  $Lipe^{+/-}$  n=6 animals). (d) Plasma glucose concentration during an 653 654 insulin tolerance test in B6D2/F1 mice fed 45% high fat diet for 3 months (n=12 animals per 655 group). (e) OUICKI and (f) mRNA level of *Elovl6* in response to refeeding in gonadal 656 adipose tissue (n=8 animals per group) in C57BL/6J mice fed 60% high fat diet for 3 months 657 (n=8 animals per group). (g-j) Experiments were carried out in wild type (WT, white bars) 658 and in mice with zinc finger nuclease-mediated deletion of Lipe exon B which promoter drives HSL expression in fat cells (*Lipe<sup>exonB-/-</sup>*, grey bars). (g) mRNA levels of transcripts 659 660 containing different exons encoding HSL in inguinal adipose tissue (n=12 animals per group). 661 (h) Western blot analysis of adipose tissue HSL protein content (10  $\mu$ g total protein) (WT n=7 animals; *Lipe<sup>exonB-/-</sup>* n =5 animals). GAPDH was used as Western blot loading control. Size 662 663 markers (in kDa) are shown on illustrative Western blot panel. (i) Plasma glucose 664 concentration and area under the curve (AUC) during a glucose tolerance test (WT n=7 animals, Lipe<sup>exonB-/-</sup> n=5 animals) in mice fed 60% high fat diet for 3 weeks and (j) mRNA 665 level of adipose tissue *Elovl6* (WT n=5 animals, *Lipe<sup>exonB-/-</sup>* n=6 animals). Data are mean 666 667 ±sem. Statistical analysis was performed using Mann and Whitney's test (a-c, h-j), unpaired 668 Student's t test (e-g) or two-way ANOVA with Bonferroni's post-hoc tests (d). Statistical 669 tests were two-sided. \*P<0.05 compared to control.

670

Figure 3. ELOVL6 has a positive effect on insulin signaling in adipocytes. (a, b) Experiments
were carried out in control (white bars, siCTR), single HSL (grey bars, siHSL), single
ELOVL6 (light orange bars, siELOVL6) or dual HSL/ELOVL6-deprived (dark orange bars,
siHSL/siELOVL6) hMADS adipocytes in basal (-) and insulin-stimulated (+, 100nM)
conditions. Insulin signaling evaluated by activating phosphorylation of IRS1 (pY612) (n=7

676 biologically independent samples per group) (Insulin stimulation: P=0.0238) (a) and AKT 677 (pS473) (n=7 biologically independent samples per group) (Insulin stimulation: P<0.0001) 678 (b). (c) Insulin signaling evaluated by activating phosphorylation of AKT (pS473) in wild 679 type (WT, white bars, n=4 animals) and *Elovl6* null (*Elovl6-/-*, light orange bars, n=3 animals) 680 mice injected with a bolus of insulin (Insulin stimulation: P<0.0001). Size markers (in kDa) 681 are shown on illustrative Western blot panels. (d, e) Plasma glucose concentration during an 682 insulin tolerance test (n=9 animals per group) (d) and gonadal adipose tissue *Elovl6* mRNA 683 levels in response to refeeding (e) in DBA/2J (white bars, n=6 animals) and C57Bl/6J (light 684 green bars, n=5 animals) mice. (f, g) Glucose disposal rate (GDR) (f) and mRNA level of 685 *ELOVL6* in visceral adipose tissue (g) from lean healthy (LE, white bars, n=13 individuals) 686 and obese women with metabolic syndrome (MS, light red bars, n=15 individuals). (h, i) M-687 value (h) and normalized *ELOVL6* mRNA level (i) in subcutaneous adipose tissue of obese 688 women before and two years after bariatric surgery (n=14 individuals). Data are mean  $\pm$ sem. 689 Statistical analysis was performed using paired (a, b, d) and unpaired (c) two way ANOVA 690 with Bonferroni's post hoc tests, unpaired Student's t test (f), Mann and Whitney's test (e, g), and Wilcoxon's test (h, i). Statistical tests were two-sided. \*P<0.05, \*\*P<0.01, \*\*\*P<0.001 691 compared to control condition or other mouse strain. In cell experiments, <sup>\$\$</sup>P<0.01, 692 693 <sup>\$\$\$</sup>P<0.001 compared to HSL-deprived adipocytes.

694

Figure 4. Oleic acid content in PL and plasma membrane fluidity mediates ELOVL6 positive effect on insulin signaling. (a-h) Experiments were carried out in control (white bars, siCTR), single HSL (grey bars, siHSL), single ELOVL6 (light orange bars, siELOVL6) or dual HSL/ELOVL6-deprived (dark orange bars, siHSL/siELOVL6) hMADS adipocytes. (a, b) Fatty acid composition in TG (a) and PL (b) (n=6 biologically independent samples per group). (c-f) hMADS adipocytes were treated with vehicle (DMSO), 1µM of ELOVL6

Morigny, Houssier et al.

701	inhibitor (ELOVL6i) or 75nM of SCD inhibitor (SCDi) for 48h. Fatty acid ratios (n=6 for
702	ELOVL6i and n=5 for SCDi biologically independent samples per group) (c,e) and insulin
703	signaling evaluated by activating phosphorylation of AKT (pS473) in basal (-) and insulin-
704	stimulated conditions (+,100nM) (n=4 biologically independent samples per group for
705	ELOVL6i and SCDi) (Insulin stimulation: P<0.0001) (d,f). DMSO-treated adipocyte values
706	are common to panels d and f and, Supplementary Fig. 1e. (g, h) hMADS were treated with
707	vehicle (V), 100µM (O100) or 500µM (O500) of oleic acid for 48h. Oleic acid levels in PL
708	(n=5 biologically independent samples per group) $(g)$ and insulin signaling evaluated by
709	activating phosphorylation of AKT (pS473) (n=5 biologically independent samples per group)
710	in basal (-) or insulin-stimulated (+, 100nM) conditions (Insulin stimulation: P=0.0003) (h).
711	For panels <b>d</b> , <b>f</b> and <b>h</b> , cropped images of vehicle and treatment lanes originate from the same
712	blot. Size markers (in kDa) are shown on illustrative Western blot panels. (i-l) Experiments
713	were carried out in control hMADS adipocytes expressing green fluorescent protein (GFP)
714	(white bars, Adeno-CTR) or overexpressing human ELOVL6 and GFP (avocado bars, Adeno-
715	ELOVL6). (i, j) Fatty acid ratio (n=8 biologically independent samples per group) (i) and
716	activating phosphorylation of IRS1 (pY612) in basal (-) and insulin-stimulated conditions (+,
717	100nM) (n=8 biologically independent samples per group) (Insulin stimulation: P<0.0001) (j).
718	(k, l) FRAP experiments using fluorescent cholera toxin B (Alexa555-CTxB) (n=5
719	independent experiments). (k) Representative confocal microscope image showing GFP and
720	Alexa455-CTxB at room temperature of a successfully transduced hMADS adipocyte. Scale
721	bar, 50 $\mu$ m. (1) Calculated mobile fraction (white bar, n=17 analyzed cells; avocado bar, n=16
722	analyzed cells). Data are mean ±sem. Statistical analysis was performed using Wilcoxon's test
723	(a,b), paired (c-f, h, j) and unpaired (d) two way ANOVA with Bonferroni's post hoc tests,
724	Friedman's with Dunn's post hoc tests (g), paired Student's t test (i) and Mann and Whitney's
725	test (I). Statistical tests were two-sided. *P<0.05, **P<0.01, ***P<0.001 compared to control.

<sup>\$\$\$</sup>P<0.01, <sup>\$\$\$\$</sup>P<0.001 compared to HSL-deprived adipocytes. <sup>#</sup>P<0.05, <sup>##</sup>P<0.01 compared to</li>
HSL- and ELOVL6-deprived adipocytes.

728

729 Figure 5. The glucose-sensitive transcription factor, ChREBP, mediates the beneficial effect 730 of diminished HSL expression on glucose metabolism and insulin signaling in adipocytes. (a-731 e) Experiments were carried out in control (white bars, siCTR), single HSL (grey bars, 732 siHSL), single ChREBP (light brown bars, siChREBP) or dual HSL/ChREBP-deprived (dark 733 brown bars, siHSL/siChREBP) hMADS adipocytes in basal (-) and insulin-stimulated (+, 734 100nM) conditions. (a) Glucose transport using radiolabelled 2-deoxyglucose (n=12 735 biologically independent samples per group) (Insulin stimulation: P<0.0001). (b, c) de novo lipogenesis using radiolabelled glucose (n=9 biologically independent samples per group) 736 737 (Insulin stimulation: P=0.0002) (b) or radiolabelled acetate (n=6 biologically independent 738 samples per group) (Insulin stimulation: P=0.0014) (c). (d, e) Insulin signaling evaluated by 739 activating phosphorylation of IRS1 (pY612) (n=8 biologically independent samples per 740 group) (Insulin stimulation: P=0.0245) (d) and AKT (pS473) (n=8 biologically independent 741 samples per group) (Insulin stimulation: P < 0.0001) (e). Size markers (in kDa) are shown on 742 illustrative Western blot panels. (f-h) Experiments were carried out in control (white bars, 743 siCTR) and ChREBP-deprived (light brown bars, siChREBP) hMADS adipocytes. (f, g) Fatty 744 acid composition in TG (f) and PL (g) (n=8 biologically independent samples per group). (h) 745 mRNA levels of lipogenic enzymes (n=6 biologically independent samples per group). (i) 746 mRNA levels of lipogenic enzymes in inguinal adipose tissue of wild type (WT, white bars, 747 n=7 animals) and *ChREBP* null mice (*Mlxipl-/-*, light brown bars, n=6 animals). (j,k)748 Experiments were carried out in control (white bars, siCTR) and HSL-deprived (grev bars, 749 siHSL) hMADS adipocytes. (j) Induction of mRNA levels of ChREBPa and ChREBP $\beta$  (n=8 750 biologically independent samples per group) and ( $\mathbf{k}$ ) ChREBP recruitment on ELOVL6 751 ChoRE (n=3 independent experiments). (l, m) Correlations between mRNA levels of 752 *ELOVL6* and *ChREBP* $\beta$  in hMADS adipocytes (n=64 biologically independent samples) (I) 753 and in human subcutaneous adipose tissue (n=31 individuals) (m). (n, o) mRNA levels of 754 *ChREBP* $\beta$  (n=7 biologically independent samples per group) (n) and *ELOVL6* (n=7) 755 biologically independent samples per group) (o) in human subcutaneous adipose tissue in 756 basal condition or during hyperglycemic-hyperinsulinemic clamp. Data are mean ±sem. 757 Statistical analysis was performed using paired two way ANOVA with Bonferroni post hoc 758 tests (a-e), paired Student's t test (f, g, j), Wilcoxon's test (h, n, o), Mann and Whitney's test 759 (i) and linear regression (l, m). Statistical tests were two-sided. \*P<0.05, \*\*P<0.01, \*\*\*P<0.001 compared to control. <sup>\$</sup>P<0.05, <sup>\$\$</sup>P<0.01, <sup>\$\$\$</sup>P<0.001 compared to HSL-deprived 760 adipocytes. <sup>#</sup>P<0.05, <sup>##</sup>P<0.01 compared to ChREBP-deprived adipocytes. 761

762

763 Figure 6. HSL inhibits ChREBP activity through protein-protein interaction. (a) 764 Representative image of immunocomplexes between immobilized FLAG-ChREBPa and 765 recombinant HSL (Rec.HSL) (n=3 independent experiments). (b) Representative surface 766 plasmon resonance assay sensorgram showing the binding of HSL to ChREBP. Purified 767 ChREBP (220RU) was first injected on a sensorchip with immobilized anti-ChREBP 768 antibody. Following ChREBP binding, PR65a (no signal) and HSL (35RU) were 769 consecutively injected (n=3 independent experiments). (c) Endogenous interaction between 770 HSL and ChREBP in human adipocytes (n=3 biologically independent samples per group). 771 Anti-ChREBP antibody was used for immunoprecipitation (IP). Normal Rabbit IgG antibody 772 was used as negative control. (d) Endogenous interaction between HSL and ChREBP in white adipose tissue of  $Lipe^{+/-}$  (+/-) and wild type (+/+) mice (n=4 animals per group). Anti-773 774 ChREBP antibody was used for immunoprecipitation. Rabbit IgG antibody was used as 775 negative control.  $\beta$ -actin was used as Western blot loading control. (e) In situ proximity

776 ligation assays (red signals) performed with anti-HSL and anti-ChREBP antibodies (PLA 777 HSL/ChREBP) and corresponding image under visible light (Phase) in control (siCTR) and 778 HSL-deprived (siHSL) hMADS adipocytes. Nuclei were labelled in blue using DAPI. 779 Representative image (6 independent experiments). Scale bars, 50µm. (f) Immunodetection of 780 ChREBP (red) in control (siCTR) and HSL-deprived (siHSL) hMADS adipocytes. 781 Representative image (4 independent experiments). Nuclei were labelled in blue using DAPI. 782 Scale bars,  $50\mu m$ . (g) ChREBP $\alpha$  protein levels in nuclear extracts from control (siCTR) and 783 HSL-deprived (siHSL) hMADS adipocytes (n=8 biologically independent samples per 784 group). (h) ChREBP $\alpha$  protein levels in nuclear extracts from white adipose tissue of wild type (WT, n=8 animals) and  $Lipe^{+/-}$  (n=9 animals) mice. (i) Luciferase assays following 785 786 transfection in HEK-293 cells of carbohydrate-responsive elements (ChoRE) fused to the 787 luciferase gene along with expression vectors for ChREBP and HSL. ChoRE activity was 788 measured in HEK-293 cells transfected with empty plasmid (pcDNA), ChREBP and different 789 concentrations of HSL expression plasmids under low (5mM, G5) (n=6 biologically 790 independent samples per group) and high (25mM, G25) glucose concentrations (n=4 791 biologically independent samples per group). (j) HSL and ChREBPa immunocomplexes in 792 HEK-293 cells transfected with empty plasmid (pcDNA3), FLAG-ChREBP, full lengh HSL 793 (HSL) or short form HSL (HSL-S) expression plasmids. Anti-FLAG antibody was used for 794 immunoprecipitation.  $\beta$ -actin was used as Western blot loading control (n=3 independent 795 experiments) (k,l) Effect of overexpression of the short inactive form of HSL (HSL-S) in 796 hMADS adipocytes. Experiments were carried out in control (siCTR, white bars) and HSL-797 deprived (siHSL, grey bars) hMADS adipocytes overexpressing green fluorescent protein 798 (GFP, Ad-CTR) or the short inactive form of HSL (Ad-HSL-S). (k) mRNA levels of *ELOVL6* 799 (n=10 biologically independent samples per group). (I) Activating phosphorylation of IRS1 800 (pY612) in basal (-) and insulin-stimulated (+, 100nM) conditions (n=6 biologically

- 801 independent samples per group, Insulin stimulation: P<0.0001). Size markers (in kDa) are
- shown on illustrative Western blot panels. Data are mean  $\pm$  sem. Statistical analysis was
- 803 performed using paired Student's t test (g), Mann and Whitney's test (h) or paired two-way
- 804 ANOVA with Bonferroni's post-hoc tests (i, k, l). Statistical tests were two-sided. \*P<0.05,
- \*\*P<0.01 \*\*\*P<0.001 compared to ChREBP condition (i) or control adipocyte (l). <sup>\$</sup>P<0.05,
- 806 <sup>\$\$\$</sup>P<0.001 compared to pcDNA condition (i) or siHSL/Ad-CTR adipocytes (k, l).
- 807

808 METHODS

809 General experimental approaches. No samples, mice, human research participants and data 810 points were excluded from the reported analysis. Randomization was not performed. Analyses 811 were not blinded except when noted below. Detailed information and description of common 812 techniques are described in Supplementary Methods as indicated below.

## 813 Culture of human adipocytes and in vitro measurements.

814 Culture of adipocytes. hMADS cells were expanded in DMEM 5.5 mM glucose (Lonza) 815 supplemented with 10% fetal bovine serum (Lonza), 2 mM L-glutamine (Invitrogen), 10 mM 816 HEPES buffer (Lonza), 50 units/ml of penicillin (Invitrogen), 50 mg/ml of streptomycin 817 (Invitrogen), supplemented with 2.5 ng/ml of fibroblast growth factor 2 (Sigma). At 818 confluence, fibroblast growth factor 2 was removed from proliferation medium. On the next 819 day (day 0), the cells were incubated in differentiation medium (DMEM/Ham's F-12 medium 820 containing 7.8 mM glucose, HEPES, L-glutamine, penicillin/streptomycin, 10 µg/ml of 821 transferrin (Sigma), 10nM of insulin (Sigma), 0.2 nM triiodothyronine (Sigma), 100 µM 3-822 isobutyl-1-methylxanthine (Sigma), 1 µM dexamethasone (Sigma), and 100 nM rosiglitazone 823 (Sigma)). At days 3 and 10, respectively, dexamethasone and 3-isobutyl-1-methylxanthine, 824 and then rosiglitazone were removed from culture medium. The experiments were carried out 825 between days 12 and 15.

For primary culture and differentiation of human preadipocytes, subcutaneous adipose tissue samples were obtained from 5 women (age  $39 \pm 9$  years; BMI  $28 \pm 4$  kg/m<sup>2</sup>) undergoing elective plastic surgery in the abdominal or dorsal region at Rangueil Hospital, Toulouse, France. Adipose tissue was cleaned from blood vessels and fibrous material, minced into pieces and digested in 1 volume of collagenase I (300 units/ml, Sigma) for 90 min in 37 °C shaking water bath. Digested tissue was filtered through 250 µm strainer, diluted with PBS/gentamycin and centrifuged at 1300 rpm for 5 min. Pellet was incubated in erythrocyte lysis buffer for 10 min at room temperature. Cells were filtered, centrifuged, resuspended in
PM4 medium with 132 nmol/L insulin for differentiation and collected at day 13 <sup>51,52</sup>. The
study was approved by the Ethics Committee of Toulouse University Hospitals (Comité de
Protection des Personnes Sud Ouest et Outre Mer 2, DC-2014-2039). The volunteers signed
informed consent for anonymous use of samples.

HEK293 and HepG2 cell cultures. See Supplementary Methods.

RNA interference. RNA interference was achieved by small interfering RNA (siRNA).
Briefly, on day 7 and day 4 of differentiation respectively, hMADS and primary
preadipocytes were detached from culture dishes with trypsin/EDTA (Invitrogen) and
counted. Control small interfering RNA against Green Fluorescent Protein (siCTR) and genespecific siRNA for HSL, ChREBP, ELOVL6 and ATGL (Eurogentec) were delivered into
adipocytes using a microporator (Invitrogen) with the following parameters: 1,100 V, 20 ms,
1 pulse. The targeted sequences are provided in Supplementary Methods.

Adenoviral infection. Adenoviruses encoding under the control of a cytomegalovirus promoter, ELOVL6 (ADV-207862), the short form of HSL, both in tandem with GFP, or GFP alone (catalog No. 1060) were obtained from Vector Biolabs. Adenoviral particles (multiplicity of infection, 200) were added in the culture medium for 24 hours at day 11-12 of hMADS cell differentiation. Medium was changed and experiments were carried out 48 hours

851 later.

852 Plasmid transfection. See Supplementary Methods.

853 Oleic acid supplementation in human adipocytes. See Supplementary Methods.

Treatments with enzyme inhibitors. For FAS, SCD and ELOVL6 inhibition, hMADS adipocytes were respectively treated with 1 $\mu$ M of compound AZ12756122 (ex 117 from WO2008075070A1, synthesized at AstraZeneca), 75nM of A939572<sup>24</sup> (Tocris Biosciences) and 1w<sup>23</sup> (provided by AstraZeneca) in culture medium for 48 hours. To study the effect of

- bioactive FA on the induction of ChREBP, cells were treated for 8h with 10µM of triacsin C
- 859 (Sigma), an inhibitor of acyl-CoA synthase, in the culture medium.
- 860 Gene expression analysis. See Supplementary Methods.

861 Characterization of human ChREBPβ-specific exon. See Supplementary Methods.

- 862 Western blot analysis. See Supplementary Methods.
- Metabolic measurements. Triacylglycerol hydrolase activity was measured on cell extracts <sup>14</sup>. 863 864 For other metabolic measurements, insulin was removed from culture medium the day before 865 the assay. To determine glucose uptake, cells were incubated 50 min at 37°C with or without 100 nM insulin. Then, 125 µM of cold 2-deoxy-Dglucose and 0.4 µCi 2-deoxy-D-[<sup>3</sup>H] 866 867 glucose (Perkin Elmer) per well were added for 10 min incubation. Culture plates were put on 868 ice and rinsed with 10 mM glucose in ice-cold PBS and then with ice-cold PBS. Cells were 869 scraped in 0.05N NaOH, and radioactive 2-deoxy-D-glucose uptake was measured by liquid 870 scintillation counting of cell lysate. To determine glucose oxidation, cells were incubated for 871 3 h in Krebs Ringer buffer supplemented with 2% BSA, 10 mM HEPES, 2 mM glucose, and 1  $\mu$ Ci D-[<sup>14</sup>C(U)]glucose (PerkinElmer) with or without 100 nM insulin. A 2x2 cm Whatman 872 3M paper was placed on top of each well and soaked with 120 µL NaOH 1N. After 873 incubation, filter-trapped <sup>14</sup>CO<sub>2</sub> was measured by liquid scintillation counting. Medium was 874 acidified with 1M sulfuric acid and medium <sup>14</sup>CO<sub>2</sub> was trapped by benzethonium hydroxide, 875 during 2 h incubation. Benzethonium-trapped <sup>14</sup>CO<sub>2</sub> was measured by liquid scintillation 876 877 counting. Specific activity was counted and used to determine the quantity of oxidized 878 glucose equivalent. To assess glucose incorporation into FA, cells were then washed twice in 879 PBS and then scraped in STED. Neutral lipids were extracted in methanol/chloroform (1:2). 880 Organic phase was dried under nitrogen and hydrolyzed in 1mL 0.25N NaOH in 881 methanol/chloroform (1:1) for 1 h at 37°C. The solution was neutralized with 500 µL 0.5N 882 HCl in methanol. FAs and glycerol were separated by adding 1.7 mL chloroform, 860 µL

water, and 1 mL methanol/chloroform (1:2). Incorporation of <sup>14</sup>C into FAs was measured by 883 884 liquid scintillation counting of the lower phase. Specific activity was counted and used to 885 determine the quantity of incorporated glucose equivalent. De novo lipogenesis was also measured using acetic acid-sodium salt-[1-<sup>14</sup>C] (PerkinElmer). Cells were incubated for 3h in 886 887 Krebs buffer supplemented with 10mM HEPES, 2mM glucose, 2%BSA and 2uCi/mL of 888 radiolabelled acetate stimulated with or without 100nM insulin. Cells were then washed twice 889 and harvest in PBS/SDS 0.1%. Neutral lipids were extracted in methanol/chloroform (1:2) method. Incorporation of <sup>14</sup>C into neutral lipids was measured by liquid scintillation counting 890 891 of lower phase. Results from metabolic measurements were normalized to total protein 892 content of cell extracts.

893 ELOVL6 activity. Fatty acid elongation activity was measured in crude microsomal extracts from hMADS adipocytes <sup>41</sup>. Briefly, cells were washed with PBS, scraped in 3 ml of ice-cold 894 250m M sucrose, Hepes 20 mM, EDTA 1 mM, pH 7.5 and dounce-homogenized. 895 896 Homogenate was centrifuged 1000 g at 4°C for 7 min. Supernatant was collected and 897 centrifuged at 2000 g at 4°C for 30 min. Supernatant was collected and centrifuged at 17000 g 898 at 4°C for 1 hour. The resultant pellet was suspended in 50 µl of 100 mM Tris-HCl, pH 7.4 899 and used for fatty acid elongation activity after determination of protein concentration. ELOVL6 activity was essayed by the measurement of [2-<sup>14</sup>C]malonyl-CoA (Perkin Elmer) 900 incorporation into exogenous palmitoyl-CoA <sup>53</sup>. ELOVL6 inhibitor (1µM of compound 1w <sup>23</sup>) 901 902 was preincubated 30 min at 37°C with microsomal protein before addition of reaction 903 mixture. Incubation was stopped by adding 0.2 ml of 5M KOH, 10% methanol and saponified 904 at 65°C for 1h. Then the samples were cooled and acidified with 0.2 ml of ice-cold 5N HCl 905 and 0.2 ml of ethanol. Free fatty acids were extracted from the mixture three times with 1 ml 906 of hexane, 2% acetic acid. The pooled hexane fractions were dried under nitrogen and after 907 addition of 3 ml of scintillation cocktail, the radioactivity incorporated was counted. Blanks

Morigny, Houssier et al.

908 were carried out in parallel reactions incubated without microsomal fractions. ELOVL6 909 activity obtained by subtracting [ $^{14}$ C]malonyl-CoA molecules incorporated into fatty acids in 910 the absence of inhibitor to the values in the presence of the ELOVL6 inhibitor.

911 Chromatin immunoprecipitation assays. Human adipocyte cells ( $10^7$  cells per condition) were 912 fixed with 1% formaldehyde for 15 min and guenched with 0.125 M glycine. Chromatin was 913 isolated by the addition of lysis buffer, followed by disruption with a Dounce homogenizer. 914 Lysates were sonicated and the DNA sheared to an average length of 300-500 bp. Genomic 915 DNA (Input) was prepared by treating aliquots of chromatin with RNase, proteinase K and 916 heat for de-crosslinking, followed by ethanol precipitation (Active Motif Inc.). Pellets were 917 resuspended and the resulting DNA was quantified on a NanoDrop spectrophotometer. 918 Extrapolation to the original chromatin volume allowed quantitation of the total chromatin 919 yield. Aliquots of chromatin (30 µg) were precleared with protein A agarose beads 920 (Invitrogen). Genomic DNA regions of interest were isolated using an antibody against 921 ChREBP (Novus, cat# NB400-135). Positive and negative controls were designed by Active 922 Motif Inc. Complexes were washed, eluted from the beads with SDS buffer, and subjected to 923 RNase and proteinase K treatment. Crosslinks were reversed by incubation overnight at 65 C, 924 and ChIP DNA was purified by phenol-chloroform extraction and ethanol precipitation. 925 Quantitative PCR reactions were carried out in triplicate using SYBR Green Supermix (Bio-926 Rad, Cat # 170-8882) on a CFX Connect<sup>™</sup> Real Time PCR system. Positive and negative 927 control sites were tested for each factor as well as the sites of interest. The resulting signals 928 were normalized for primer efficiency by carrying out qPCR for each primer pair using input 929 DNA (pooled unprecipitated genomic DNA from each sample).

930 Cellular subfractionation. Nuclear and cytosolic fractions from hMADS adipocytes were
931 prepared using Nuclear Extract Kit (40010) from Active Motif. Cells were rinsed with PBS
932 and immediately scrapped into 1X Hypotonic Buffer. For adipose tissue, tissues were ground

933 in liquid nitrogen and lysed using the NE-PER nuclear and cytoplasmic extraction reagent kit 934 (Thermoscientific, 78835). Subsequent steps followed the manufacturer's protocol. Anti-935 histone H3 (4499, Cell Signaling Technology), anti-lamin A/C (4777, Cell Signaling 936 Technology) and  $\alpha$  tubulin (T5168, Sigma) antibodies were used to analyze the efficiency of 937 cellular fractionation.

938 Fatty acid composition of TG and PL. Cells were scraped in PBS and then mixed with 939 methanol supplemented with butylated hydroxytoluene (BHT) 0.001%. Lipid extraction was 940 performed with a chloroform/methanol mixture (1:1) and KCl (0.5 M) after centrifugation 941 (2500rpm, 10min). PL and TG were isolated by thin-layer chromatography on silica glass 942 plates (Merck) using petroleum ether/diethyl ether/acetic acid (80:20:1) as the mobile phase. 943 FA methyl esters were generated by transmethylation of the glycerolipids in methanol with 5 944 % acetyl chloride at 60°C for 1 hour, extracted 2 times by isooctane. Analysis was carried out 945 with a gas chromatograph (Shimadzu GC 2100) equipped with a CP-Wax 58 capillary 946 column, 50 m in length, 0.25-mm external diameter and 0.2-µm thickness of the stationary 947 phase (Varian Inc.), with helium 1 mL/min as carrier gas. Programmed temperature 948 vaporization (PTV system) injector and flame ionization detector were used. Results are 949 expressed in percentage of total FA contained in the sample.

950 Fatty acid composition in phospholipid classes. See Supplementary Methods.

951 Measurement of glycerol and NEFA in culture medium. See Supplementary Methods.

Fluorescence recovery after photobleaching (FRAP). Cells were labeled for 15 min with 1 $\mu$ g/ml Alexa 555-labeled Cholera ToxinSubunit B (CTxB Molecular Probes) at 4°C, then washed three times in chilled medium supplemented with 25 mM HEPES buffer, pH 7.4. LSM780 confocal microscope, equipped with a high sensitive 32 channel GaAsP detectors, operated with Zen Black software, coupled to a DPSS-laser (561 nm, maximum power 20 mW) was used for excitation with a detection bandwidth of 571-624 nm (Carl Zeiss). All

958 experiments were done at room temperature (22°C). Cells were observed using a Plan-959 Apochromat 63X NA 1.4 oil immersion objective, and the pixel dwell was set to the optimal 960 value of 1.92  $\mu$ s. The fluorescence intensity of three regions of interest of 6.4  $\mu$ m×3.2  $\mu$ m was 961 measured: the photobleached area, a region within the cell that was not photobleached to 962 check for overall photobleaching and cell position fluctuation and the background. After 10 963 prebleach scans (one scan every 200 ms) at 1% maximal laser power to determine initial 964 fluorescence intensity, one photobleaching scan was performed at 100% laser power. Post 965 bleach fluorescence recovery was then sampled at 1% laser power for 150 s. FRAP data analysis was done using the method described by Bonneau et al. 54. 966

Immunoprecipitation. HEK293T cells were harvested in a lysis buffer containing 3% NaCl
5M, 5% TrisHCl 1M (pH 7.5), 1% EDTA 500mM, 1.338% PPiNa and 0.02% NaF,
supplemented with 1% Triton X-100 (Sigma), 2% 50X protease inhibitor cocktail (Roche)
and 1% 1mM orthovanadate (Sigma). 1 mg of proteins was immunoprecipitated overnight at
4°C, with 40µL of anti-FLAG M2 magnetic beads (Sigma). Beads were gently centrifuged for
1 min and washed with the lysis buffer before elution in Laemmli buffer.

973 For immunoprecipitation between purified proteins, FLAG-tagged ChREBP was expressed in 974 HEK293T cells. Cells were harvested in lysis buffer described above. 300 µg of proteins was 975 immunoprecipitated overnight at 4°C with 40µL of anti-FLAG M2 magnetic beads. Beads 976 bound with ChREBP were washed with the lysis buffer and incubated with 1 µg of human 977 recombinant HSL (Cayman) in 350 µl of lysis buffer for 3h at 4 °C with gentle rocking. The 978 beads were washed 3 times with lysis buffer.

For endogenous co-immunoprecipitation in hMADS adipocytes, cells were lysed for 15min in
1X hypotonic buffer (Active Motif) with 4% 25X protease inhibitor cocktail (Roche) and
1mM orthovanadate (Sigma). Cell debris and fat was discarded after 12700rpm centrifugation
at 4°C for 15min. Preclearing was performed at 4°C for 30min using 50µL protein G and 4µg

control rabbit (2729, Cell Signaling Technology) or mouse (sc-2025, Santa Cruz) IgG. Beads
were discarded and supernatants were incubated with 4µg anti-ChREBP (NB400-135, Novus)
ou 2µg anti-HSL (sc-74489, Santa Cruz Biotechnology) for 90 min at 4°C. As negative
control of immunoprecipitation, 4µg control rabbit (2729, Cell Signaling Technology) or 2µg
mouse (sc-2025, Santa Cruz) IgG were used. Protein A/protein G (50:50) magnetic beads
were added for 1h at 4°C. Beads were washed in cold PBS with 4% 25X EDTA and 1mM
orthovanadate.

990 For ChREBP immunoprecipitation in mouse white adipose tissue, fat was cut in small pieces 991 and lysed during 2h in 20 mM Tris/HCl, 150 mM NaCl, 0.5% NP-40 and 992 protease/phosphatase inhibitors; pH 8. Following centrifugation at 15000g for 20 min at 4°C, 993 fat layer was removed before collecting the supernatant. For each immunoprecipitation, 0.8 to 994 1 mg of protein was precleared with 50 µl of Protein A Dynabeads (ThermoFisher) for 1h at 995 4°C, then incubated overnight at 4°C with 40µl Protein A dynabeads coupled with 5µg Rabbit 996 IgG or ChREBP antibody (Novus). Beads were washed 4 time with lysis buffer prior elution 997 in 2X Laemmli buffer.

998 In situ proximity ligation assay and immunofluorescence. In situ proximity ligation assay was 999 performed using Duolink In Situ reagents (Sigma). Cells and pieces of subcutaneous adipose 1000 tissue were fixed with 4% paraformaldehyde (Sigma) and permeabilized 15 min at room 1001 temperature with 0.2% Triton X-100 (Sigma). Incubation of antibodies, ligation of 1002 oligodeoxynucleotides and amplification were performed following manufacturer's 1003 instructions. The following primary antibodies were incubated overnight at 4°C: anti-HSL 1004 (murine antibody, sc-74489, Santa Cruz Biotechnology), anti-ATGL (mouse antibody, NBP2-1005 59390, Novus), anti-AKT (mouse antibody, 2920, Cell Signaling Technology) and anti-1006 ChREBP (rabbit antibody, NB400-135, Novus). The same antibodies were used in 1007 immunofluorescence assays. Anti-mouse (Alexa-fluor 488-conjugated, A21202, and Alexa-

Morigny, Houssier et al.

fluor 546-conjugated, A10036, Invitrogen) and anti-rabbit (Alexa-fluor 546-conjugated, Invitrogen) secondary antibodies were incubated at 1/300 for 45min. Neutral lipids were stained using Bodipy (4-3922, Life Technologies) for 30min. Nucleus labeling was performed using Hoescht (33342, 5mg/mL, Invitrogen) for 5 min. Confocal microscopy was performed using Zeiss LSM780. Image processing was similar for all conditions. The same settings were applied to entire images.

1014 Surface Plasmon Resonance assays. All binding studies based on surface plasmon resonance 1015 technology were performed on BIAcore T200 optical biosensor instrument (GE Healthcare). 1016 Immobilization of anti-ChREBP antibody (NB400-135, Novus) was performed by the Fc 1017 region to the chip surface using native Protein A sensorchip in PBS-P+ buffer (20mM Phosphate Buffer pH 7.4, 2.7mM Kcl, 137mM NaCl, and 0.05% surfactant P20) (GE 1018 1019 Healthcare). Immobilization step were performed at a flow rate of 5 µl/min with a final 1020 concentration of 2µg/ml. Total amount of immobilized antibody was 11000-12000RU. Then 1021 all injection steps were performed at a flow rate of 20µl/min.Channel Fc1 was used as a 1022 reference surface for non-specific binding measurements.

- 1023 Luciferase activity. See Supplementary Methods.
- 1024

Animal studies. No randomization and blinding was performed. Animals from several litters
were used in each protocol to avoid litter-to-litter variation.

Mouse models. Targeted disruption of the *Lipe* gene and generation of *Lipe*<sup>+/-</sup> mice have been described elsewhere <sup>13</sup>. Before euthanasia, mice were fasted for 24h or refed for 18h supplemented with 20% glucose in drinking water. To create transgenic mice with specific deletion of *Lipe* exon B, mRNA coding for zinc finger nucleases targeting specifically HSL (CompoZr<sup>TM</sup> Custom Zinc Finger Nucleases, CSTZFN-1KT, Sigma) was injected into pronuclei of one-cell embryos from female B6D2/F1 mice. Homozygous mice (*Lipe<sup>exonB-/-</sup>* 

Morigny, Houssier et al.

registered as B6D2-Lipe<sup>em1Land</sup> mice) were obtained. Full description of the model will be 1033 1034 published elsewhere. The specific inhibitor of HSL (BAY 59-9435) was synthesized by NoValix (Illkirch, France)<sup>55</sup>. Transgenic mice were fed high fat diet (60% or 45% kcal fat, 1035 1036 respectively, D12492 and D12451 from Research Diets) for indicated times. In 1037 pharmacological studies, C57BL/6J male mice (12-15 weeks-old, Janvier Laboratories) were 1038 treated orally with DMSO or HSL inhibitor (70mg/kg once daily) for 11 days. Eight week-old 1039 DBA2/J and C57BL6/J male mice (Charles River) were fed high fat diet (60% kcal fat, 1040 D12492 from Research Diets) for 6 weeks before sacrifice. Mice were housed and 1041 manipulated according to Inserm guidelines and European Directive 2010/63/UE in the local 1042 animal care facility (agreements A 31 555 04 and C 31 555 07). Protocols were approved by 1043 the French Ministry of Research following review by local ethical committee (CEEA122).

In studies on ChREBP null mice, 10 to 12 week-old male and female *Mlxipl* global knockout mice <sup>56</sup> and wild-type littermates were maintained in a 12-h light/dark cycle with water and chow diet (65% carbohydrate, 11% fat, and 24% protein). For fasting-refeeding experiment, mice were either fasted for 24h (fasted group) or refed for 18h on chow diet and had access to drinking water with 20% glucose, following a 24h fast (Refed group). Mice were housed and manipulated according to Inserm guidelines and European Directive 2010/63/UE in the local animal care facility (agreement A751320). Protocols were approved by the French Ministry of

1051 Research following review by local ethical committee (CEEA34).

Mice homozygous for a deletion in *Elovl6* and their wild-type littermates were phenotyped on a C56BL6/J background <sup>57</sup>. The research has been regulated under the Animals (Scientific Procedures) Act 1986 Amendment Regulations 2012 following ethical review by the University of Cambridge Animal Welfare and Ethical Review Body (AWERB).

1056 Gene and protein expression analyses. See Supplementary Methods.

1057 Measurement of fasting glucose and insulin. See Supplementary Methods.

## Morigny, Houssier et al.

1058 Glucose and insulin tolerance tests and insulin bolus injection. See Supplementary Methods.

1059 Euglycemic-hyperinsulinemic clamp. See Supplementary Methods.

Human research. Nature of the groups was blinded to the investigator performing geneexpression experiments.

1062 Women with differing obese and metabolic status. Participating women (lean group mean age 1063  $37 \pm 16$  years; obese with metabolic syndrome group mean age,  $49 \pm 11$  years) were 1064 scheduled to have abdominal surgery (laparoscopic or laparotomic cholecystectomy and gastric banding) <sup>58</sup>. During the surgical procedure, samples of visceral adipose tissue were 1065 1066 obtained by surgical excision. Euglycemic hyperinsulinemic clamp was performed at rest 1067 after an overnight fast. Each subject gave written informed consent and the study was approved by the Ethics Committee of the Third Faculty of Medicine, Charles University, 1068 1069 Prague.

1070 Hyperglycemic hyperinsulinemic clamp. The 8 participating men were  $23 \pm 3$  years-old (BMI,  $23 \pm 2 \text{ kg/m}^2$ ). The hyperglycemic hyperinsulinemic clamp was a modification of the 1071 1072 hyperglycemic method used by Del Prato et al. combined with the original hyperinsulinemic clamp described by Defronzo<sup>59,60</sup>. For hyperglycemia, the objective was to increase plasma 1073 1074 glucose 5.5 mmol/l above fasting level by infusing 20% dextrose in two phases: 1) bolus dose 1075 to increase glycemia to the desired target and 2) continuous infusion dose adjusted every 5-101076 min according to measured plasma glucose to maintain glycemia at the desired target. To 1077 obtain hyperinsulinemia, insulin was co-infused at the rate of 75 mU/m<sup>2</sup> min for 180 min. The 1078 study was approved by the Ethics Committee of University of Montreal. The volunteers gave 1079 their written consent after being informed of the nature, purpose, and possible risks of the 1080 study.

1081 Morbidly obese subjects undergoing bariatric surgery. This cohort has in part been described 1082 before <sup>61</sup>. In brief, 14 obese women (BMI>35 kg/m<sup>2</sup>; age,  $48 \pm 9$  years) referred to the

hospital for gastric by-pass surgery (Roux-en-Y) were investigated before surgery and 2 years post-operatively. According to self-report, body weight had been stable ( $\pm$  2 kg) for at least 3 months prior to both investigations. The study was approved by the regional ethics board in Stockholm and registered at clinicaltrials.gov as NCT01785134. Subjects were randomized to omentectomy or not and this was blinded to investigators and patients. Procedure was explained in detail to each women and written informed consent was obtained.

1089 Gene expression analysis. See Supplementary Methods.

1090

1091 **Statistical analysis.** Results from biological replicates were expressed as mean  $\pm$  SEM. 1092 Statistical analyses were performed using GraphPad Prism (GraphPad Software v.5.0). 1093 D'Agostino and Pearson omnibus normality test was used to test normality. Fischer test was 1094 used to test for equality of variances. Data were Log transformed when appropriate to reach 1095 normality and uniform distribution. Statistical tests were two-sided. Paired or unpaired 1096 Student's t tests, Wilcoxon's test and, Mann and Whitney's test were performed to compare 1097 two conditions. Paired or unpaired one-way ANOVA and Friedman's tests were performed 1098 and followed respectively by Bonferroni's and Dunn's post hoc tests to determine differences 1099 between several groups. Paired or unpaired two-way ANOVA with Bonferroni's post hoc 1100 tests were used to compare two variables. Linear regression was used to test association 1101 between two variables.

1102

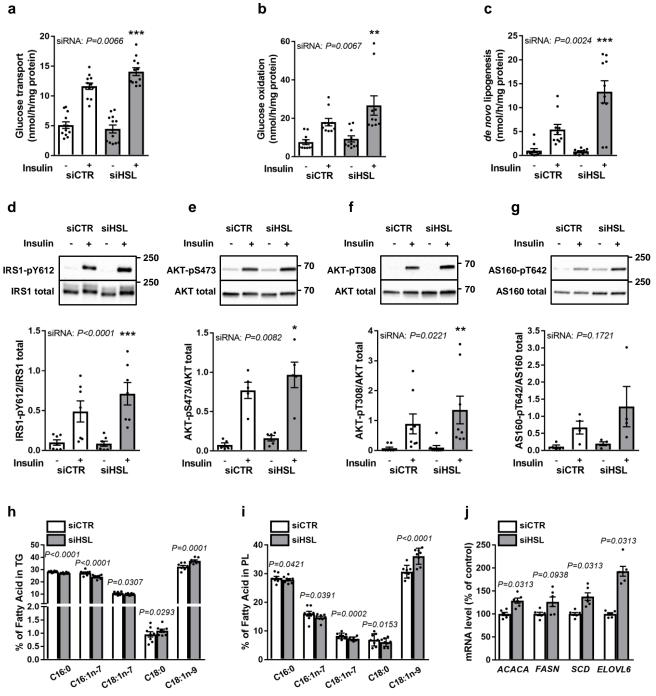
**Data availability statement.** The data that support the plots within this paper and other findings of this study are available from the corresponding author upon reasonable request.

1105

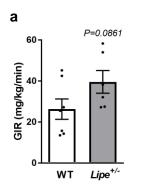
## 1106 METHODS-ONLY REFERENCES

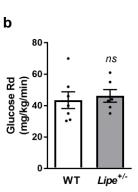
- Skurk, T., Ecklebe, S. & Hauner, H. A novel technique to propagate primary human
  preadipocytes without loss of differentiation capacity. *Obesity (Silver Spring)* 15,
  2925-2931 (2007).
- 1110 52. Rossmeislova, L., *et al.* Weight loss improves the adipogenic capacity of human
  1111 preadipocytes and modulates their secretory profile. *Diabetes* 62, 1990-1995 (2013).
- 1112 53. Moon, Y.A., Shah, N.A., Mohapatra, S., Warrington, J.A. & Horton, J.D.
  1113 Identification of a mammalian long chain fatty acyl elongase regulated by sterol
  1114 regulatory element-binding proteins. *J Biol Chem* 276, 45358-45366 (2001).
- 1115 54. Bonneau, L., *et al.* Plasma membrane sterol complexation, generated by filipin,
  1116 triggers signaling responses in tobacco cells. *Biochim Biophys Acta* 1798, 2150-2159
  1117 (2010).
- 1118 55. Langin, D., *et al.* Adipocyte lipases and defect of lipolysis in human obesity. *Diabetes*1119 54, 3190-3197 (2005).
- 1120 56. Iizuka, K., Bruick, R.K., Liang, G., Horton, J.D. & Uyeda, K. Deficiency of
  1121 carbohydrate response element-binding protein (ChREBP) reduces lipogenesis as well
  1122 as glycolysis. *Proc Natl Acad Sci U S A* 101, 7281-7286 (2004).
- 1123 57. Tan, C.Y., *et al.* Brown Adipose Tissue Thermogenic Capacity Is Regulated by 1124 Elovl6. *Cell Rep* **13**, 2039-2047 (2015).
- 1125 58. Klimcakova, E., *et al.* Worsening of obesity and metabolic status yields similar
  1126 molecular adaptations in human subcutaneous and visceral adipose tissue: decreased
  1127 metabolism and increased immune response. *J Clin Endocrinol Metab* 96, E73-82
  1128 (2011).
- 1129 59. DeFronzo, R.A., Tobin, J.D. & Andres, R. Glucose clamp technique: a method for
  1130 quantifying insulin secretion and resistance. *Am J Physiol* 237, E214-223 (1979).

- 1131 60. Del Prato, S., *et al.* Characterization of cellular defects of insulin action in type 2 (non1132 insulin-dependent) diabetes mellitus. *J Clin Invest* 91, 484-494 (1993).
- 1133 61. Dahlman, I., *et al.* The fat cell epigenetic signature in post-obese women is
  1134 characterized by global hypomethylation and differential DNA methylation of
  1135 adipogenesis genes. *Int J Obes (Lond)* **39**, 910-919 (2015).
- 1136

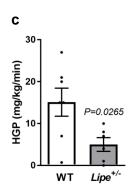


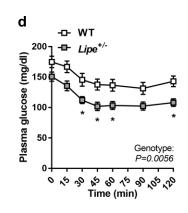
а



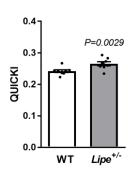


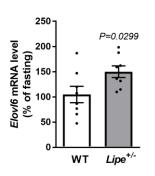
f



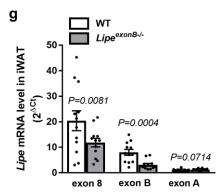




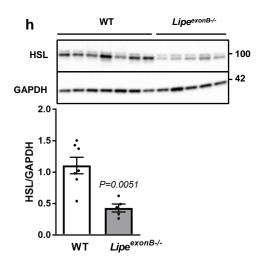


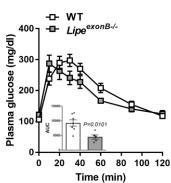


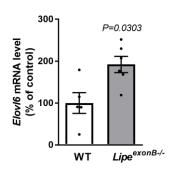
i

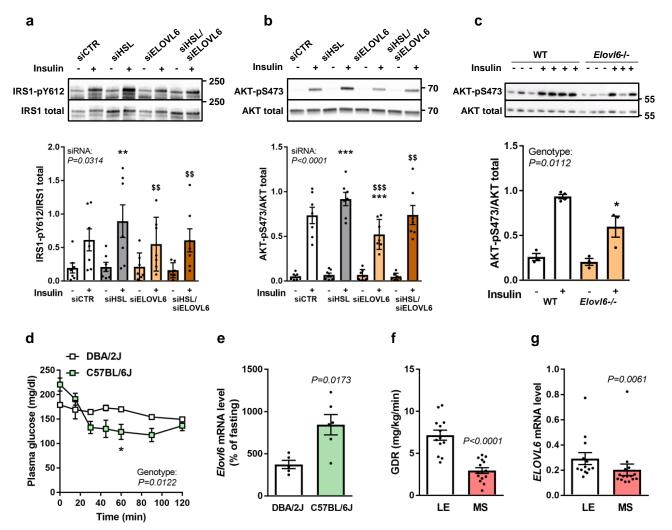


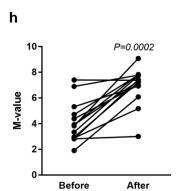
j

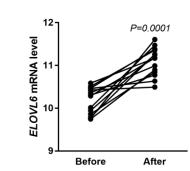




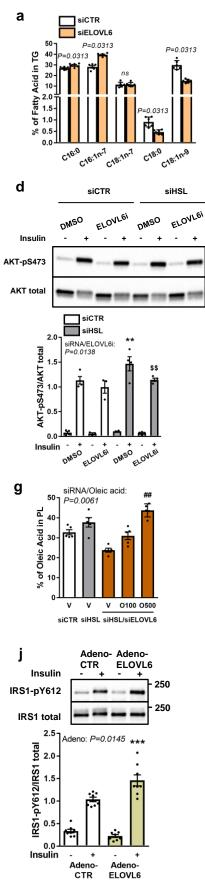






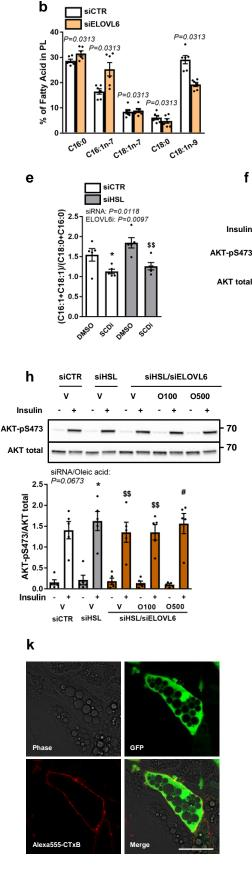


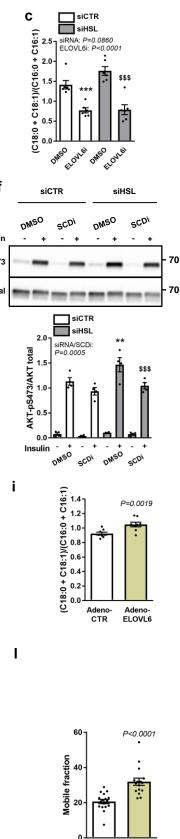
i



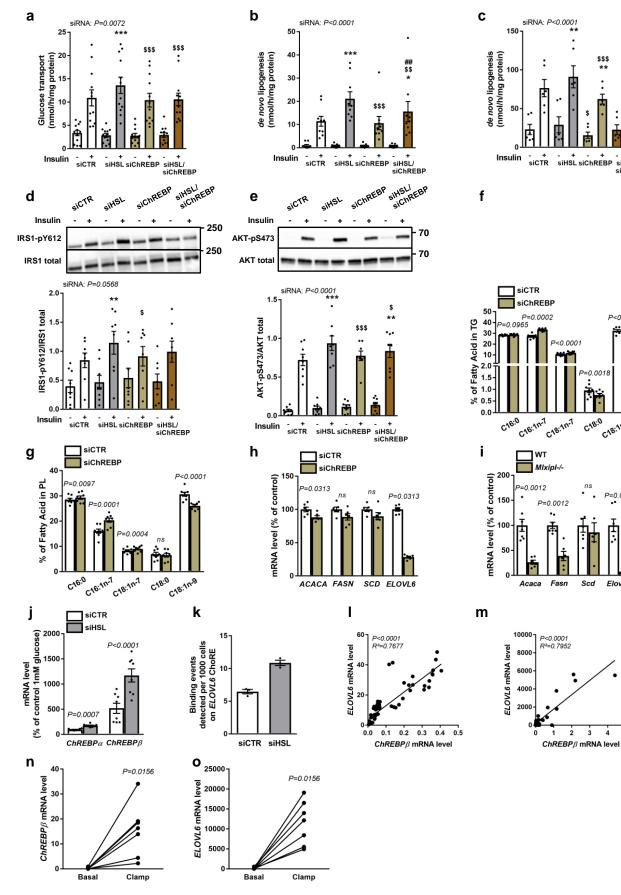
70

70





Adeno- Adeno-CTR ELOVL6



\$\$ #

siHSL/ siChREBP

P<0.0001

C18:111.9

P=0.0012

Elovl6

3 4 5

\$\$\$

